The relative importance of wind and hydroclimate drivers in modulating windblown dust emissions in Earth system models

Xinzhu Li[1], Longlei Li[2], Yan Feng[3], and Xin Xi[1]

[1]Department of Geological and Mining Engineering and Sciences, Michigan Technological University, Houghton, MI, USA
[2]Department of Earth and Atmospheric Sciences, Cornell University, Ithaca, NY, USA
[3]Environmental Science Division, Argonne National Laboratory, Lemont, IL, USA

Correspondence: Longlei Li (ll859@cornell.edu) and Xin Xi (xinxi@mtu.edu)

Abstract. Windblown dust emissions are governed by near-surface wind speed and soil erodibility, the latter influenced by hydroclimate conditions and land use. Accurate representations of the influence of these drivers in Earth system models is critical for reproducing historical dust variability and projecting dust responses to future climate and land-use changes. Here we evaluate the model consistency in simulating the interannual variability of dust emissions and quantify the variance explained by wind speed and hydroclimate drivers within 21 Earth system models and three climate zones (hyperarid, arid and semiarid). In the hyperarid zone, the models exhibit poor agreement in dust variability, with only 10% out of 210 pairwise comparisons showing significant positive correlations. In arid and semiarid zones, the models display a dipole pattern driven by a "double-edged sword" effect of land surface memory: models with coherent hydroclimate variability show improved agreement, whereas those with divergent hydroclimate representations show increased disagreement. Most models capture the dominant influence of wind speed on dust emissions in hyperarid areas except GFDL-ESM4 and CESM2-CAM-Kok, which display large spatial variability and anomalously high sensitivity to soil moisture and precipitation, respectively. Incorporating the Kok et al. (2014) scheme in CESM and E3SM generally amplifies the dust sensitivity to hydroclimate drivers and reduces the wind contribution to explained variance, e.g., from 56% to 46% for CESM and from 86% to 75% for E3SM in the arid zone. These findings underscore the need to improve the representations of near-surface winds in hyperarid areas and hydroclimate and land surface processes in arid and semiarid areas to reduce model uncertainties in dust emission estimates.

1 Introduction

Windblown dust aerosol is an essential element of the Earth's biogeochemical cycle, but has become a global concern due to its wide-ranging impacts on the climate, ecosystems, agriculture, and society. Dust emission is modulated by a number of atmospheric and land surface variables which can be grouped into three broad drivers: sediment supply, sediment availability, and wind erosivity, which collectively determine the timing, location, duration, intensity, and impacts of dust events (Xi, 2023). The most abundant *sediment supply* is typically found in low relief areas with thick layers of fine, unconsolidated materials generated via weathering, fluvial, and/or aeolian processes (Bryant, 2013). The *sediment availability* for airborne dust production is strongly affected by soil moisture and surface armoring (e.g., vegetation, soil crust, non-erodible coarse particles) which determine the minimum or *threshold wind velocity* required to initiate dust mobilization (Bullard et al., 2011).

To initiate dust emission, near-surface winds must be strong enough to exceed the threshold wind velocity. As a result, the *wind erosivity* is dominated by infrequent, high wind events which generate sufficient drag to mobilize soil particles via saltation and sandblasting mechanisms. Depending on the relative importance of the three drivers, dust emission may fall into one of three distinct regimes: *supply-limited*, where a lack of suitable-sized sediments restricts dust emission; *availability-limited*, where fine sediments are present but protected against erosion; and *transport capacity-limited*, where sediments are dry and exposed but near-surface winds are too weak to mobilize the particles.

The three dust emission drivers have been incorporated in global aerosol-climate models and Earth system models (ESMs) to capture the environmental controls on the dust cycle. Dust emission schemes in many ESMs use a time-invariant dust source function to represent the spatially varying sediment supply, with high values generally associated with topographic depressions containing abundant alluvial or lacustrine deposits (Ginoux et al., 2001; Prospero et al., 2002; Zender et al., 2003). These areas are generally assumed to have an unlimited sediment supply, without accounting for depletion or replenishment over time (Zhang et al., 2016a). The sediment availability is strongly coupled with the hydroclimate variability in ESMs. Specifically, a bare soil fraction scaling factor is often used to exclude non-erodible surfaces covered by snow or vegetation. Vegetation also increases surface roughness and reduces the wind stress acting on erodible surfaces, which can be represented by a drag partitioning scheme (Marticorena and Bergametti, 1995; Shao et al., 2011). In addition, ESMs incorporate the role of soil moisture in enhancing the threshold wind velocity or suppressing dust emissions if the soil water content exceeds a given threshold (e.g., Fécan et al., 1999). Finally, ESMs parameterize the horizontal dust flux as the third or fourth power of wind speed once the threshold wind velocity is reached. This nonlinear relationship, combined with the skewed distribution of wind speeds, reflect the dominant contributions of rare, high-wind events to global dust emissions (Cowie et al., 2015; Bergametti et al., 2017). Representing dust-producing wind events in ESMs remains a major challenge, since peak-wind generation mechanisms (such as convective downdrafts) often occur at spatial scales smaller than the typical grid spacing of ESMs (Cakmur et al., 2004; Grini et al., 2005; Ridley et al., 2013; Zhang et al., 2016b).

The Aerosol Comparisons between Observations and Models (AeroCom) initiative and Coupled Model Intercomparison Project (CMIP) have facilitated the intercomparison of ESMs in simulating the global dust cycle (Textor et al., 2006; Huneeus et al., 2011; Kim et al., 2014; Wu et al., 2020; Gliß et al., 2021; Zhao et al., 2022; Kim et al., 2024). Generally, the modern-day dust aerosol column burden is reasonably constrained by ground- and satellite-based aerosol optical depth (AOD) observations over continental outflow areas, resulting in better model agreement compared to dust emission and deposition estimates. Knippertz and Todd (2012) suggested that model tunings to match satellite observations, e.g., via the use of dust source functions, induce a compensational effect between dust emission and deposition, both of which lack observational constraints at global scales. Indeed, previous AeroCom and CMIP model intercomparisons consistently show large discrepancies in the global total and regional distribution of dust emissions (Huneeus et al., 2011; Wu et al., 2020; Gliß et al., 2021; Zhao et al., 2022). While most ESMs roughly capture the annual cycle of dust over major source regions, they struggle in reproducing the dust interannual variability and relationships with wind speed and soil bareness (Pu and Ginoux, 2018; Evan et al., 2014; Evan, 2018; Wu et al., 2018). Recent studies suggested that all CMIP models failed to capture the large increase of global dust burden since preindustrial times, likely due to inaccurate model representations of historical climate and land-use changes and/or the

dust sensitivity to these changes Kok et al. (2023); Leung et al. (2025). Together, these studies underscore the persistent uncertainties and limited predictive capability of ESMs in simulating the response of windblown dust emissions to hydroclimate variability and land surface changes.

The model discrepancies can be explained, at least in part, by the choice of dust emission schemes. Earlier-generation schemes relied on empirical, temporally-invariant dust source functions to shift emissions towards satellite-observed hotspot regions (Ginoux et al., 2001; Zender et al., 2003), whereas newer schemes adopt more mechanistic approaches that account for sediment availability as a function of land surface conditions, thereby eliminating the need for dust source functions (Kok et al., 2014b). These process-based schemes also introduce more realistic parameterizations of sandblasting efficiency to represent the momentum transfer from salting soil grains to the entrainment of fine particles into the atmosphere (Zender et al., 2003; Kok et al., 2014b). With improved model physics, process-based schemes usually involve more extensive input parameters with greater uncertainties. The choice of wind speed also varies: some schemes use 10-m wind speeds for simplicity, while others use friction velocity, which better captures the wind stress acting on soil surfaces but requires information on surface roughness. Because surface roughness length is poorly constrained by observations, models employ varying assumptions and tunings to account for its effects on dust emission (e.g., Peng et al., 2012; Albani et al., 2015; Tegen et al., 2019).

Even with the same dust scheme, ESMs can diverge substantially due to differences in model configurations (e.g., horizontal resolution, vertical levels), parameter tunings, and coupled parameterizations. For instance, the bare soil fraction is determined from land type, vegetation fraction, and snow areal extent, all of which may differ between ESMs. In particular, vegetation cover may be prescribed from a fixed climatology or simulated interactively. Further discrepancies may result from differences in soil properties (e.g., hydraulic conductivity), soil column structure (e.g., number and thickness of layers), and hydrologic processes (e.g., precipitation, runoff, evaporation), which ultimately determine the water content of top soil layers and consequently the threshold wind velocity. The soil moisture effect on threshold wind velocity is also treated inconsistently, e.g., in calculating the residue level below which soil moisture is assumed to have no effects on dust emission (e.g., Fécan et al., 1999; Evans et al., 2016; Volodin and Kostrykin, 2016). Moreover, ESMs employ different parameterizations for planetary boundary layer and subgrid processes, which affect the momentum transfer from the atmosphere to the surface. Because of the strong coupling between dust emission and boundary layer and land surface processes, it is not surprising that dust emission estimates are strongly model-dependent.

While past studies have documented the large model diversity in the climatological dust cycle (e.g., Pu and Ginoux, 2018; Wu et al., 2020; Zhao et al., 2022; Aryal and Evans, 2023), key questions remain as to whether current ESMs consistently capture the temporal variability of historical dust emissions and their sensitivities to wind and hydroclimate drivers. Addressing these questions is essential for understanding and reducing model uncertainties in projecting dust emission responses to future changes in climate and land use. In this study, we provide a detailed assessment of the interannual variability and physical drivers of dust emissions, by quantifying the inherent relative influence of near-surface wind speed and hydroclimate conditions in modulating the dust variability within a suite of state-of-the-art ESMs. Compared to previous studies, we shift the focus from climatological means to temporal variability and move beyond documenting uncertainties to diagnosing their physical origins, thereby offering critical insights for improving the dust representation in ESMs.

A major challenge in evaluating dust models is the lack of direct, global observational constraints on dust emission fluxes. While satellite-derived dust optical depth and long-term surface concentration records provide valuable insights into dust variability (e.g., Prospero and Lamb, 2003; Zender and Kwon, 2005; Ginoux et al., 2012), they integrate information from emission, transport, and deposition, making it difficult to isolate the emission process (the focus of this work). Therefore, rather than validating absolute model performance against observations, we focus on diagnosing the inter-model consistency of simulated dust emission variability. Here we treat model-simulated dust emission flux as an unobservable, model-specific quantity, which is characterized by a dynamic range defined by the internal model variability, parameterizations, parameter uncertainties, and model configurations. This approach is analogous to Koster et al. (2009)'s view of root-zone soil moisture and reflects the fact that model-simulated dust emission fluxes cannot be validated with field observations. While model-simulated dust emissions are essentially approximations of the true state they aim to reproduce, their true information content lie not necessarily in the absolute magnitudes but in their spatiotemporal variability and sensitivities to physical drivers. By quantifying the relative influence of wind speed and hydroclimate conditions over different climate regimes (i.e., hyperarid, arid and semiarid), this study provides new insights into model discrepancies and biases in dust emission representations.

The remainder of this paper is organized as follows. Section 2 describes the ESMs and reanalysis datasets considered in this study, and the dominance analysis technique used to quantify the joint and relative influence of dust emission drivers. Section 3 presents the intercomparison of dust interannual variability and the relative influence of wind speed and hydroclimate conditions. The conclusions are summarized in Section 4.

2 Data and Approach

2.1 ESMs and reanalysis products

Table 1 summarizes the ESMs and reanalysis products analyzed in this study, which differ in model resolution, vegetation process, and dust emission parameterizations, among other aspects. Among the 21 ESMs, 18 are from the CMIP6 historical, fully-coupled experiments (1980–2014). We use the first ensemble member (r1i1p1f1) from each model, unless otherwise stated. CMIP6 consists of several model families that share common heritage but differ in physics options and configurations. For instance, two Community Earth System Model (CESM) configurations employ the dust scheme of Zender et al. (2003) (hereafter the Zender scheme) but use different atmospheric schemes: Community Atmosphere Model (CESM2-CAM-Zender) vs. Whole Atmosphere Community Climate Model (CESM2-WACCM-Zender), with major differences in the vertical extent and upper atmospheric processes. Three GISS-E2 models use the same dust scheme of Miller et al. (2006) but differ in model version (2.1 vs. 2.2) and aerosol microphysics schemes: One-Moment Aerosol (OMA; ensemble member r1i1p3f1) vs. Multi-configuration Aerosol TRacker of mIXing state (MATRIX; ensemble member r1i1p5f1) (Miller et al., 2021; Rind et al., 2020). UKESM1.0 is built upon the HadGEM3-GC3.1 general circulation model, which use the same dust scheme of Woodward (2001) but differ in parameter tunings and dust source representations (Woodward et al., 2022). Similarly, MIROC-ES2L is based on the MIROC general circulation model version 5.2 (MIROC5) (Hajima et al., 2020), while MIROC6 incorporates

Table 1. Summary of the Earth system models and aerosol reanalysis datasets considered in this study. Dust source function (DSF) column indicates whether an empirical dust source function is used. Leaf area index (LAI) column indicates whether LAI is a prognostic variable. D_m, dust particle diameter upper limit.

Model	Resolution	D_m	Wind	DSF	LAI	Dust Scheme	Reference
CESM2-CAM-Zender	0.9°×1.25°	10	u_*^3	Y	Y	Zender et al. (2003)	Albani et al. (2015)
CESM2-WACCM-Zender	0.9°×1.25°	10	u_*^3	Y	Y	Zender et al. (2003)	Gettelman et al. (2019)
CESM2-CAM-Kok	0.9°×1.25°	10	u_*^3	N	Y	Kok et al. (2014b)	Li et al. (2022)
E3SM2-Zender	1°×1°	10	u_*^3	Y	Y	Zender et al. (2003)	Feng et al. (2022)
E3SM3-Kok	1°×1°	10	u_*^3	Y	Y	Zender et al. (2003)	Xie et al. (2025)
CanESM5-1	2.8°×2.8°	Bulk	u_*^3	Y	Y	Peng et al. (2012)	Sigmond et al. (2023)
CNRM-ESM2.1	1.4°×1.4°	20	u_*^3	N	Y	Tegen et al. (2002)	Séférian et al. (2019)
EC-Earth3-AerChem	2°×3°	20	u_*^3	Y	N	Tegen et al. (2002)	Van Noije et al. (2021)
GISS-E2.1-OMA	2°×2.5°	32	u_{10}^3	Y	N	Miller et al. (2006)	Miller et al. (2021)
GISS-E2.1-MATRIX	2°×2.5°	32	u_{10}^3	Y	N	Miller et al. (2006)	Miller et al. (2021)
GISS-E2.2-OMA	2°×2.5°	32	u_{10}^3	Y	N	Miller et al. (2006)	Rind et al. (2020)
GFDL-ESM4	1°×1.25°	20	u_*^3	Y	Y	Ginoux et al. (2001)	Shevliakova et al. (2024)
HadGEM3-GC31	0.6°×0.8°	63	u_*^3	Y	N	Woodward (2011)	Roberts et al. (2019)
UKESM1.0	1.25°×1.9°	63	u_*^3	N	Y	Woodward (2001)	Woodward et al. (2022)
INM-CM5.0	1.5°×2°	Bulk	u_*^4	N	N	Volodin and Kostrykin (2016)	Volodin (2022)
IPSL-CM6A-LR	1.26°×2.5°	Bulk	u_{10}^3	Y	Y	Balkanski et al. (2004)	Lurton et al. (2020)
MRI-ESM2.0	1.9°×1.9°	20	u_*^3	N	N	Shao et al. (1996)	Yukimoto et al. (2019)
MIROC6	1.4°×1.4°	10	u_{10}^3	N	Y	Takemura et al. (2009)	Tatebe et al. (2019)
MIROC-ES2L	2.8°×2.8°	10	u_{10}^3	N	Y	Takemura et al. (2009)	Hajima et al. (2020)
MPI-ESM-1.2	1.9°×1.9°	Bulk	u_*^3	Y	Y	Cheng et al. (2008)	Mauritsen et al. (2019)
NorESM2	0.9°×1.25°	10	u_*^3	Y	N	Zender et al. (2003)	Seland et al. (2020)
MERRA2	0.5°×0.63°	20	u_{10}^3	Y	N	Ginoux et al. (2001)	Randles et al. (2017)
JRAero	1.1°×1.1°	20	u_*^3	N	N	Shao et al. (1996)	Yumimoto et al. (2017)

updated physics which improved the mean climate state and internal variability relative to MIROC5 (Tatebe et al., 2019). Both MIROC-ES2L and MIROC6 adopt the dust scheme from the SPRINTARS aerosol module (Takemura et al., 2009).

In addition to the CMIP6 archive, we consider an updated CESM (2004–2013) with the dust scheme of Kok et al. (2014b) (hereafter the Kok scheme; CESM2-CAM-Kok) (Li et al., 2022), and the Energy Exascale Earth System Model (E3SM, 1980–2014) using the Zender (E3SM2-Zender) and Kok (E3SM3-Kok) schemes (Feng et al., 2022; Xie et al., 2025). The key difference between the two schemes is that the Kok scheme adopts physically based soil erodibility parameterizations and eliminates the use of empirical dust source functions unlike the Zender scheme. These paired experiments allow us to evaluate how the choice of dust schemes (Zender vs. Kok) or models (CESM vs. E3SM) affect dust emission simulations. Nonetheless, we should point out that CESM2-CAM-Kok simulates dust as mineral components with observationally constrained mineral optical properties (Li et al., 2024), whereas CESM2-CAM-Zender does not account for particle mineralogy and simulates different dust optical properties that may affect dust radiative feedback on meteorology. Also, E3SM3 includes extensive updates over E3SM2 that may affect the near-surface meteorological and land surface conditions relevant to dust emissions (Xie et al., 2025).

We further compare the ESMs with two aerosol reanalysis products: Modern-Era Retrospective Analysis for Research and Applications version 2 (MERRA2, 1980–2014) (Gelaro et al., 2017), and Japanese Reanalysis for Aerosol (JRAero, 2011–2017) (Yumimoto et al., 2017). MERRA2 is produced by the GEOS-5 data assimilation system with radiatively-coupled Goddard Chemistry Aerosol Radiation and Transport (GOCART) module. Dust emission in GOCART is represented using the Ginoux et al. (2001) scheme. JRAero is produced by the Japan Meteorological Agency MASINGAR mk-2 global aerosol transport model, which simulates dust emission using the Shao et al. (1996) energy-based scheme, same as MRI-ESM2.0 (Yumimoto et al., 2017; Yukimoto et al., 2019). The meteorological and land surface conditions in MERRA2 and JRAero are constrained by observational data assimilation, and thus are expected to better capture historical climate and land cover changes than the ESMs. MERRA2 and JRAero also benefit from assimilation of bias-corrected total AOD, which provides some constraint on the dust column burden but does not directly constrain dust emissions.

We evaluate the consistency between ESMs and reanalysis products in representing the interannual variability of total dust emission fluxes. To facilitate comparison across common dust-emitting regions, we divide global dust source areas into three climate zones: hyperarid, arid, and semiarid, based on the aridity index (AI) defined as the ratio of 1970–2000 climatological mean precipitation to potential evapotranspiration using the data from Zomer et al. (2022). The hyperarid zone is defined as $AI \leq 0.05$, arid zone as $0.05 < AI \leq 0.2$, and semiarid zone as $0.2 < AI \leq 0.5$. Using these climatologically defined zones allows us to assess model discrepancies over common dust-emitting areas. Figure 1 shows that the hyperarid zone primarily covers North Africa, Arabian Peninsula, Iranian Plateau, and Tarim Basin. Arid and semiarid zones cover other major sources, including the Sahel (North Africa), Turan Depression (Central Asia), Gobi Desert (East Asia), Thar Desert (South Asia), Kalahari Desert (Southern Africa), Chihuahua Desert (North America), Patagonia steppe (South America), and the Great Sandy and Simpson Deserts (Australia). The rationale of this climate zone-based analysis is that the relative importance of wind speed versus hydroclimate conditions is expected to depend strongly on climate regime. Specifically, hyperarid areas are expected to be dominated by permanently dry, barren surfaces with very low hydroclimate variability, and thus dust emission is primarily

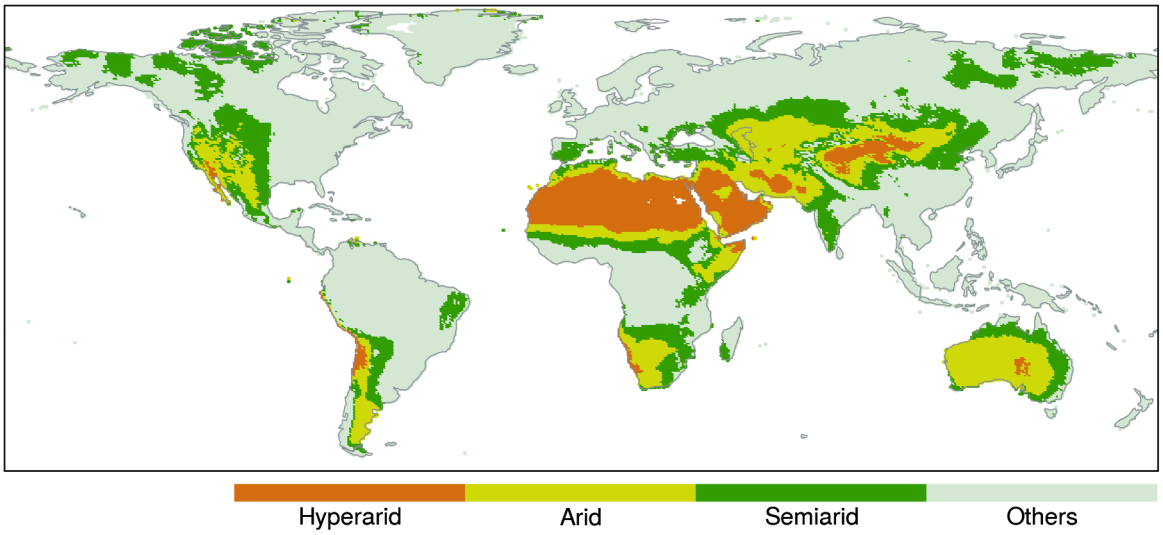

Figure 1. Definitions of hyperarid, arid, and semiarid climate zones.

controlled by wind speed. Whereas, the arid and semiarid zones are expected to exhibit increased precipitation and hydroclimate variability resulting in stronger influence on the sediment availability.

2.2 Dominance analysis technique

Past studies have used linear regression coefficients to quantify dust sensitivities to its physical drivers (e.g., Pu and Ginoux, 2016; Aryal and Evans, 2021; Zhao et al., 2022). In multiple linear regression, a regression coefficient represents the mean change in the response variable per unit change in a given predictor, holding all other predictors constant. This interpretation assumes mutual independence among predictors, an assumption that is often violated by strong correlations among hydroclimate variables. As a result, linear regression coefficients may yield misleading inference of predictor importance. Moreover, regression coefficients, standardized or not, may not provide a direct comparison of predictor influence due to the varying dynamic ranges in ESMs.

In this study, we apply the dominance analysis technique to quantify the relative influence of wind and hydroclimate drivers on dust variability. Dominance analysis quantifies the marginal contribution of each predictor to the total explained variance (R^2) in the response variable by evaluating all possible subset models ($2^p - 1$ subsets for p predictors) in a multiple linear regression framework (Budescu, 1993; Azen and Budescu, 2003). For each predictor, the method calculates its average incremental contribution to the total R^2 across all subset models of the same size (i.e., models with the same number of predictors), and then average these values to obtain the predictor's unique contribution to the total R^2. A key property of this method is that the sum of individual predictor contributions equals the R^2 of the full model (i.e., with all predictors included), thereby allowing the partitioning of explained variance among correlated predictors. The predictor-specific R^2 values can thus be interpreted

as the portions of total variance in the response variable that are uniquely and jointly attributed to each predictor, accounting for their interactions and multicollinearity.

We use the monthly total dust emission flux as the response variable and consider six predictors: 10-m wind speed, total precipitation (including liquid and solid phases), water content in the uppermost soil layer (hereafter as soil moisture), 2-m specific humidity, 2-m air temperature, and leaf area index (LAI). The total dust emission flux is a bulk quantity that represents the source strength. Although ESMs differ in how they partition the total flux into discrete particle size bins—a key factor influencing dust transport and atmospheric lifetime—we expect the size partitioning to have minimal impact on diagnosing the emission process itself, particularly its sensitivity to the selected predictors. The primary drivers of emission variability operate upstream of the size partitioning of mobilized soil particles. The six predictors are chosen because they are either directly used as input parameters in dust flux calculations or strongly correlated with dust emission intensity, as suggested in numerous studies (e.g., Engelstaedter et al., 2003; RAVI et al., 2006; Zou and Zhai, 2004; Sokolik et al., 2021; Cowie et al., 2015; Kim and Choi, 2015; Xi and Sokolik, 2015a, b; Xi, 2023). Among them, wind speed represents the wind erosivity driver, while the remaining variables collectively represent the hydroclimate effect on sediment availability.

Dominance analysis is performed for all ESMs and MERRA2 over grid cells with nonzero emissions using deseasonalized and normalized data. JRAero is excluded from the dominance analysis due to missing predictors and its short time span. We first subtract month-wise climatological means from the monthly dust fluxes and predictors, and then convert the deseasonalized data into 0–1 range via min-max normalization. For ESMs that use bare soil fraction as a scaling factor in dust flux calculations (e.g., CNRM-ESM2.1, INM-CM5.0, UKESM1.0), the dust flux is first normalized by the bare soil fraction in order to isolate the influence of the selected predictors. The grid-level total and predictor-specific R^2 values are used to assess the internal spatial variability (i.e., within each climate zone) and inter-model consistency in the total explained variance and predictor relative importance.

3 Results

3.1 Climatological distribution

Figure 2 displays the climatological mean annual dust fluxes from 21 ESMs, the model ensemble mean, and MERRA2 and JRAero datasets for the 2005–2014 period (2004–2013 for CESM2-CAM-Kok and 2011–2017 for JRAero). All datasets capture the global dust belt stretching from West Africa to East Asia, as well as the less intense sources in the Americas and Australia. E3SM3-Kok and HadGEM2-GC31 simulate the most extensive dust-emitting areas including high-latitude and subhumid areas. In contrast, CESM2-CAM-Zender, CESM2-WACCM-Zender, and NorESM2 simulate discrete and limited dust-emitting areas by excluding areas with dust source function values below 0.1. E3SM2-Zender uses the original, unmodified Zender et al. (2003) dust source function and thus produces a more spatially continuous pattern (Fig. 2e).

The global total dust flux varies greatly among the ESMs, ranging from 890 to 7727 Tg yr^{-1} with nearly an order of magnitude difference (Fig. 2a–2u). The model ensemble mean estimate is 2786 Tg yr^{-1} (Fig. 2v) with a standard deviation of 1821 Tg yr^{-1}, corresponding to a diversity of 65% (defined as the ratio of standard deviation to model ensemble mean).

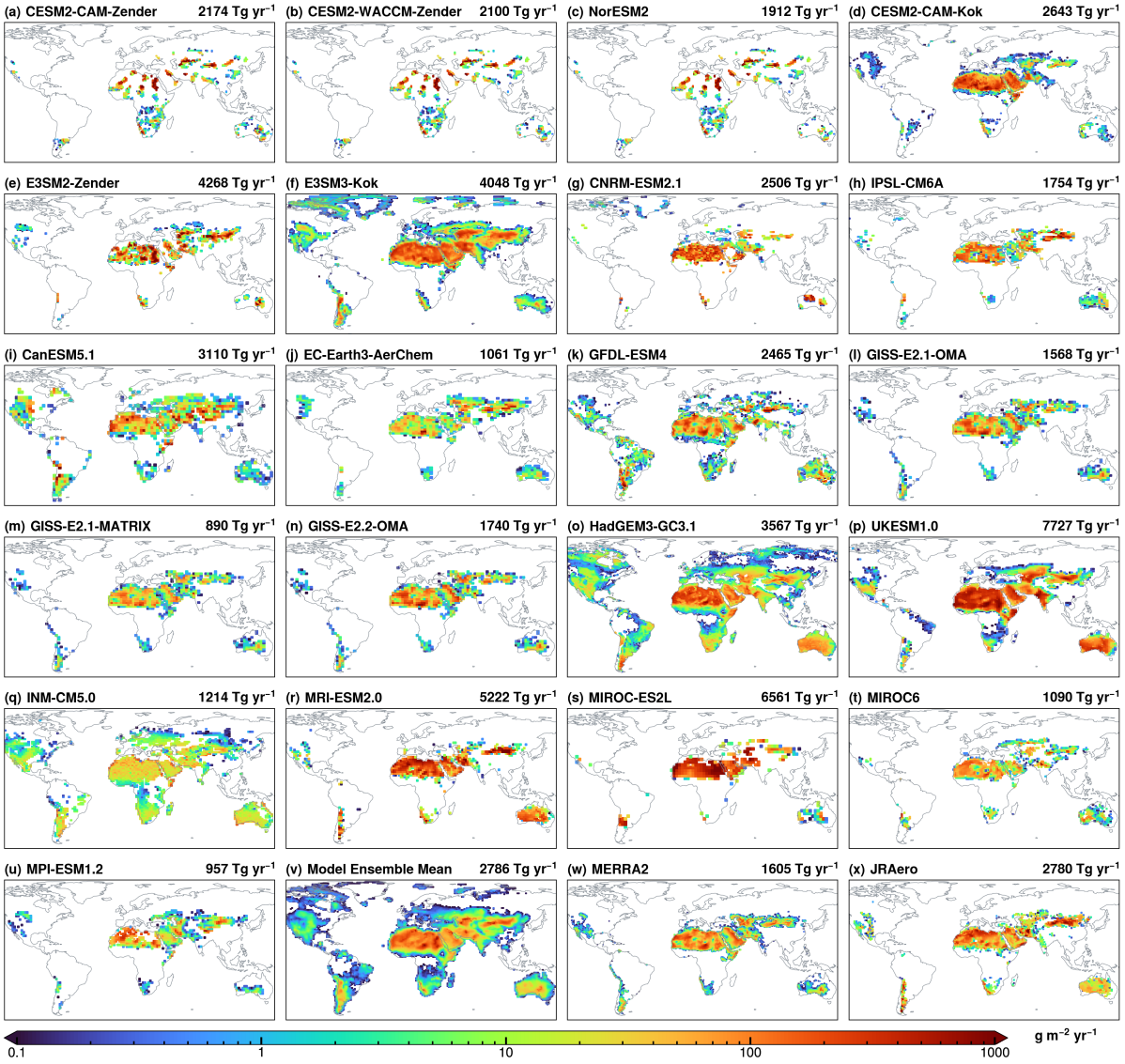

Figure 2. Climatological mean dust emission fluxes from (a–u) individual Earth system models, (v) model ensemble mean, (w) MERRA2 reanalysis, and (x) JRAero reanalysis. Global annual total dust emissions are displayed on each panel.

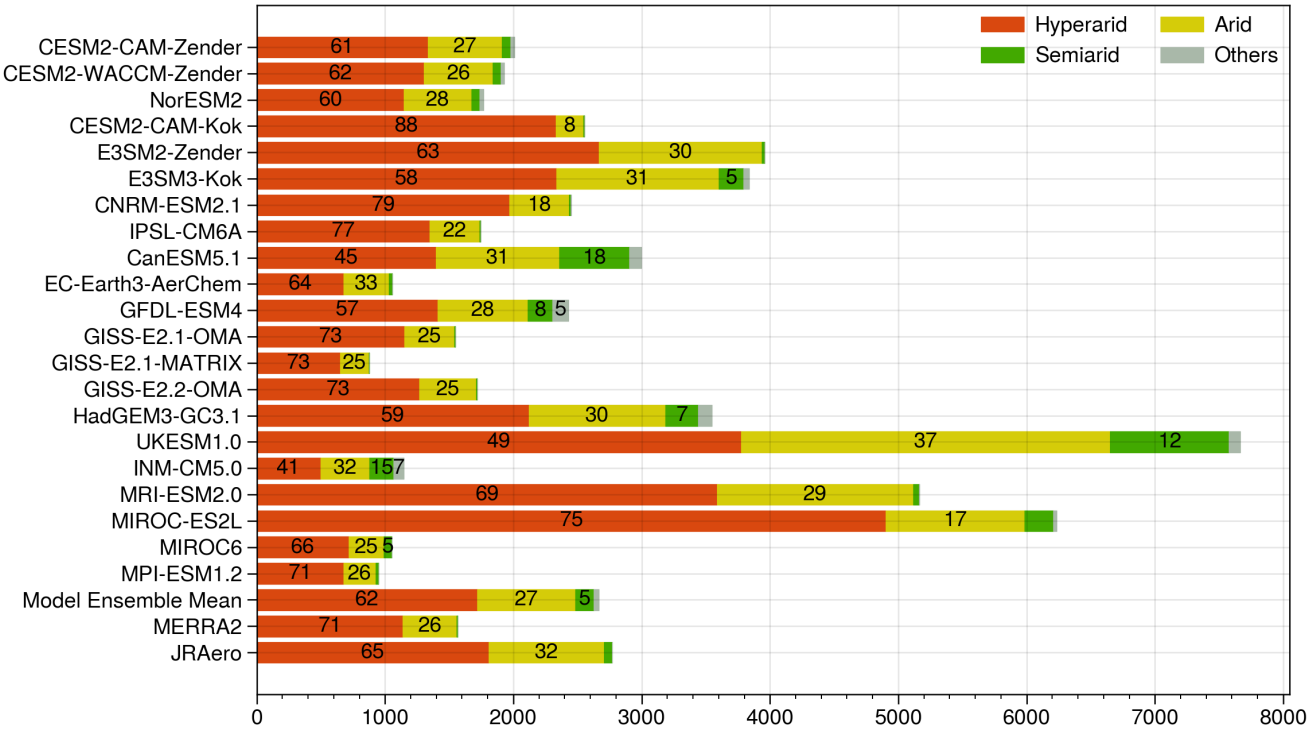

Figure 3. Contributions of different climate zones to global annual dust emissions. Numbers indicate percentages above 5%.

Based on models with a dust size upper limit of 20 μm, global dust emissions vary from 1062 to 6561 Tg yr^{-1} with a mean of 3012 Tg yr^{-1} and diversity of 51%. This uncertainty range is consistent with prior assessments. For example, Huneeus et al. (2011) compared 14 models from AeroCom Phase I and reported a global dust emission range of 500–4400 Tg yr^{-1} with a diversity of 58%. Out of the 14 models, 7 models considered particle diameters up to 20 μm and reported a flux of 980–4300 Tg yr^{-1} with a diversity of 46%. Similarly, Gliß et al. (2021) compared 14 AeroCom Phase III models and found a range of 850–5650 Tg yr^{-1} with a diversity of 64%. Wu et al. (2020) reported a range of 740–8200 Tg yr^{-1} with a diversity of 66% based on 15 CMIP5 models. Out of the 15 models, 7 models considering a diameter range of 0–20 μm yielded 740–3600 Tg yr^{-1} with a diversity of 43%. More recently, Zhao et al. (2022) compared 15 models from the CMIP6 AMIP experiment and reported a range of 1400–7600 Tg yr^{-1} with a diversity of 61%. Past studies, together with our results, indicate persistent large uncertainties in global dust emissions, despite improvements in model resolutions and physics.

The model ensemble mean global total dust flux is significantly higher than that of MERRA2 (1605 Tg yr^{-1}, Fig. 2w), but closely aligns with JRAero (2780 Tg yr^{-1}, Fig. 2x). In general, the model ensemble mean exhibits a more spatially homogeneous pattern over North Africa and Arabian Peninsula, whereas MERRA2 and JRAero display more heterogeneous and localized patterns.

Figure 3 displays the fractional contributions of different climate zones to global dust emissions. The hyperarid zone accounts for more than half of global total emissions in most ESMs except two models: CanESM5.1 and INM-CM5.0, both of which simulate relatively uniform emission patterns with less than 50% from the hyperarid zone (Fig. 2i, 2q). This may be due to known deficiencies of these two models. As noted in Sigmond et al. (2023), improper parameter tuning related to the hybridization of dust tracers caused spurious dust events and inaccurate dust distributions in CanESM5.1. An interpolation error in the bare soil fraction also distorted the model's dust source characterization, resulting in poor agreement with satellite observations (Sigmond et al., 2023). In INM-CM5.0, the vertical dust flux is calculated as a function of friction velocity only, without accounting for the dependence of threshold wind velocity on land surface conditions (Volodin and Kostrykin, 2016; Volodin, 2022). While this simplification may be appropriate for the hyperarid zone, it can introduce significant biases over arid and semiarid zones where hydroclimate conditions play an increasingly important role in dust emissions.

Over the arid climate zone, the dust emission fraction ranges from 8% (CESM2-CAM-Kok) to 37% (UKESM-1.0), reflecting substantial discrepancies among the ESMs. These discrepancies become even larger over the semiarid zone, where the contribution ranges from less than 1% to 18%. Three ESMs allocate more than 10% of dust to the semiarid zone: CanESM5.1 (18%), INM-CM5.0 (15%), and UKESM1.0 (12%). Thus, as the climate zone shifts from hyperarid to semiarid, the ESMs show larger discrepancies in their estimates of relative source strength. This climate zone-based comparison offers a first-order view of model representations of the dust sensitivity to hydroclimate conditions. Based on the model ensemble mean, global dust emissions are partitioned as 61% from hyperarid, 27% from arid, and 5% from semiarid zones. In contrast, MERRA2 and JRAero produce most dust from hyperarid and arid zones, with negligible contributions from the semiarid zone.

Among the ESMs, CESM2-CAM-Zender, CESM2-WACCM-Zender and NorESM2 produce similar total emissions and regional fractions, suggesting that the choice between CAM and WACCM has minimal influence when the same dust scheme (Zender) is used. The paired CESM and E3SM experiments show different changes in regional fractions. For instance, the hyperarid zone fraction increases from 61% in CESM2-CAM-Zender to 88% in CESM2-CAM-Kok, but slightly decreases from 63% in E3SM2-Zender to 58% in E3SM3-Kok. The GISS-E2 models show no differences in the regional distributions. However, the total emission is about 40% lower when using the MATRIX aerosol scheme. This could be due to different model tuning parameters, or underestimation of coarse dust particles (>5 μm diameter) in the MATRIX modal size distribution, as pointed out by Bauer et al. (2022). UKESM1.0 simulates nearly twice as much dust as HadGEM3-GC3.1, along with slightly more even distributions. As described in Woodward et al. (2022), UKESM1.0 is built on HadGEM3-GC3.1 but applies model tunings that enhance friction velocity and suppress soil moisture. These tunings are expected to increase the wind gustiness and soil dryness in UKESM1.0, thereby strengthening dust emissions. UKESM1.0 also excludes emissions from seasonally vegetated regions, resulting in smaller dust-emitting areas (Fig. 2p) compared to HadGEM3-GC3.1 (Fig. 2o). The three Japanese models (MRI-ESM2.0, MIROC-ES2L, and MIROC6) exhibit large differences in total emissions and, to a lesser degree, regional distributions. MRI-ESM2.0 produces similar regional fractions to JRAero but nearly twice the total emissions. Despite using the same dust scheme, MIROC-ES2L produces five times more dust than MIROC6. This discrepancy can be largely explained by the stronger winds in MIROC-ES2L, which produces 50% higher global mean wind speed than MIROC6.

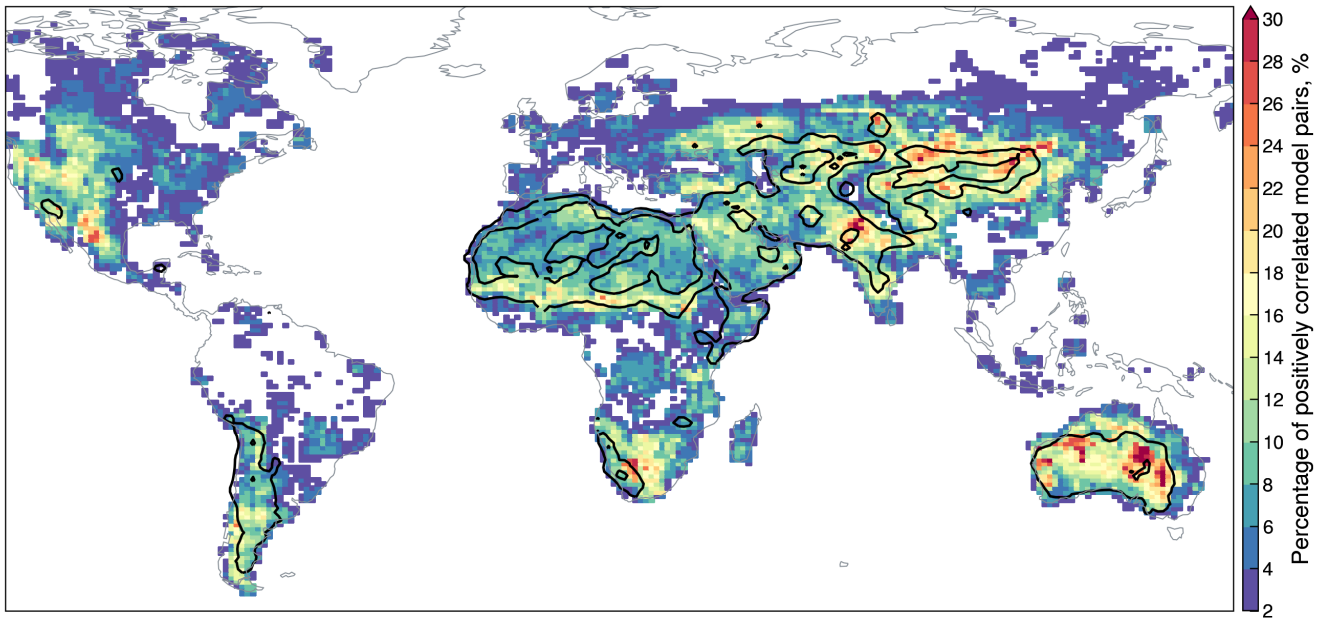

Figure 4. Percentage of statistically significant ($p \leq 0.1$), positive correlations out of every possible pairwise comparisons of monthly dust emission fluxes from 21 Earth system models. Black contours represent the model ensemble mean annual dust flux of 10 and 100 Tg yr^{-1}.

Moreover, MIROC6 prescribes non-zero LAI even in hyperarid regions, which likely further suppresses dust emissions relative to MIROC-ES2L (Hiroaki Tatebe, personal communications).

3.2 Interannual variability

This section evaluates the consistency among the ESMs in simulating the interannual variability of dust emissions. Monthly dust emission fluxes from all ESMs are first regridded to a common resolution of 0.9°×1.25° (the native grid of CESM2). To remove the influence of annual cycles, we subtract the month-wise climatological means from each grid cell, yielding deseasonalized dust emission anomalies. Spearman's rank correlation coefficients are then calculated between the deseasonalized anomalies for all possible model pairs. With 21 ESMs, this yields 210 pairwise comparisons. To quantify the extent of inter-model agreement, we calculate the percentage of model pairs that exhibit statistically significant ($p \leq 0.1$), positive correlations, which is displayed in Fig. 4. A higher percentage indicates stronger inter-model agreement in simulating the interannual variability of dust emissions.

Despite its dominant contributions to global dust emissions, the hyperarid zone shows generally poor model agreement, with less than 10% of pairwise comparisons yielding statistically significant, positive correlations. Because dust emissions from hyperarid areas are primarily controlled by wind speed, this weak agreement reflects inconsistent wind simulations in the ESMs. Indeed, we find that only 10% of model pairs produce statistically significant, positively correlated wind variability in

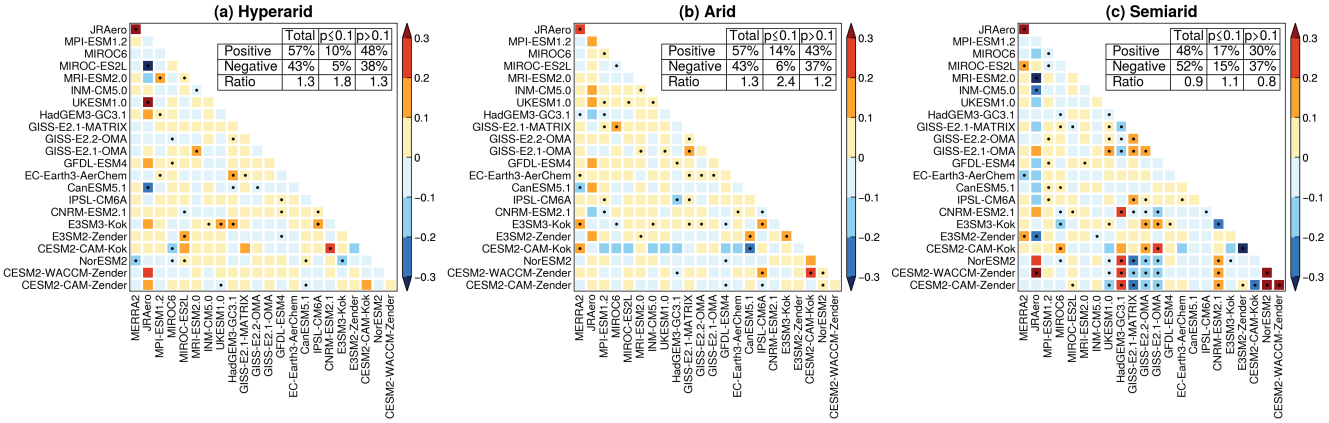

Figure 5. Spearman's rank correlation coefficients between dust emission flux anomalies averaged over hyperarid, arid, and semiarid climate zones. Dots indicate statistically significant correlations ($p \leq 0.1$). Summary tables are based on Earth system models only (MERRA2 and JRAero not included).

the hyperarid zone. Similarly, Evan (2018) reported that dust-producing winds over the Sahara are mainly driven by large-scale meteorological processes and that most CMIP5 models failed to capture the near-surface wind variability. These results suggest that accurately representing near-surface winds is critical for reducing model discrepancies in dust variability over hyperarid areas.

Compared to the hyperarid zone, arid and semiarid zones (such as the Sahel, South Asia, East Asia and Australia) exhibit significantly stronger model agreement. To illustrate how model consistency varies with climate zones, Fig. 5 presents the pairwise correlation matrices based on dust flux anomalies averaged over hyperarid, arid, and semiarid zones. The percentage of statistically significant, positively correlated model pairs increases from 10% in the hyperarid zone to 14% in the arid zone and 17% in the semiarid zone, indicating progressively higher model agreement in regions where dust emissions are increasingly influenced by hydroclimate and land surface conditions. Meanwhile, the semiarid zone exhibits a larger percentage of negatively correlated model pairs (15%) compared to hyperarid (5%) and arid (6%) zones. This dipole pattern suggests that as the climate regime transitions from hyperarid to semiarid, the ESMs exhibit both stronger agreement and worsened disagreement in simulating dust emission variability.

What causes this complex behavior? In semiarid environment such as temperate grasslands and steppes, dust emissions are strongly modulated by antecedent land surface conditions in addition to wind speed, such as precipitation, soil moisture, and vegetation growth-decay cycle, which exert strong lagged influence on the soil erodibility (Shinoda et al., 2011; Nandintsetseg and Shinoda, 2015). For example, dry anomalies during the prior wet season (e.g., reduced snowfall or rainfall, accelerated snow retreat) can subsequently suppress vegetation growth, thereby prolonging bare soil exposure and increasing wind erosion risk. This delayed dust emission response to preceding drought exemplifies the effect of land surface memory, whereby the slow adjustment of land surface states (such as soil moisture, snow cover, and vegetation) over weeks to months influences

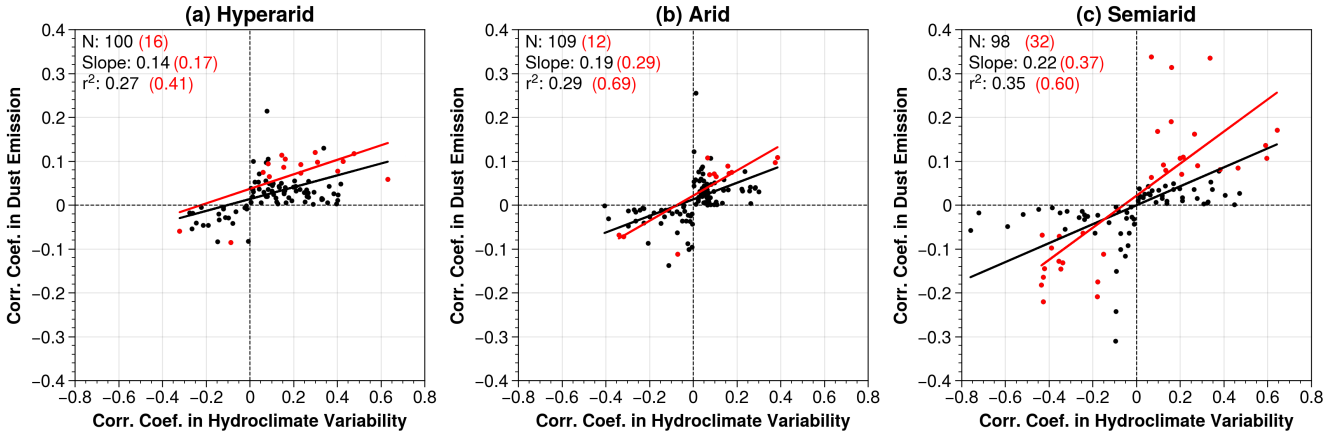

Figure 6. Statistical associations between the pairwise model correlation coefficients ($p \leq 0.1$ shown in red) in dust emission fluxes and hydroclimate variability over (a) hyperarid, (b) arid, and (c) semiarid climate zones.

subsequent dust emission long after the initial forcing (e.g., drought). Therefore, we speculate that the simultaneous increase of both model consistency and divergence from hyperarid to semiarid zones reflects a "double-edged sword" effect of land surface memory: models with coherent representations of hydroclimate variability converge in the simulated dust emission variability (i.e., more positive correlations), while those with divergent hydroclimate representations diverge in the dust variability (i.e., more negative correlations).

To verify this hypothesis, we examine the statistical association between pairwise model correlations in dust emissions and those in hydroclimate variability. Specifically, we first perform a principle component analysis (PCA) of the five hydroclimate variables (i.e., precipitation, soil moisture, specific humidity, air temperature, LAI) for the hyperarid, arid, and semiarid zones. The leading principle component (PC1), which explains at least 40% of the total variance in all zones, is used as a proxy for the dominant hydroclimate variability. Spearman's rank correlation coefficients are then calculated for all pairwise model comparisons of deseasonalized monthly PC1 values, following the same approach as in Fig. 5. Figure 6 compares the correlation coefficients for model pairs with the same sign (i.e., either both positive or both negative) in dust emission fluxes and hydroclimate PC1. The regression slope and coefficient of determination (r^2) quantify the degree of statistical association between model correlations in dust emission and hydroclimate variability. The positive association in all climate zones suggests that ESMs with stronger consensus in hydroclimate variability tend to produce more consistent dust variability, and vice versa. More importantly, both the number of significantly correlated model pairs (N) and correlation strength (slope and r^2) show significant increases from hyperarid to semiarid zones. This result supports our hypothesis regarding the dual role of land surface memory: it enhances agreement among ESMs with coherent hydroclimate representations, while simultaneously exacerbating disagreement among those with divergent hydroclimate variability.

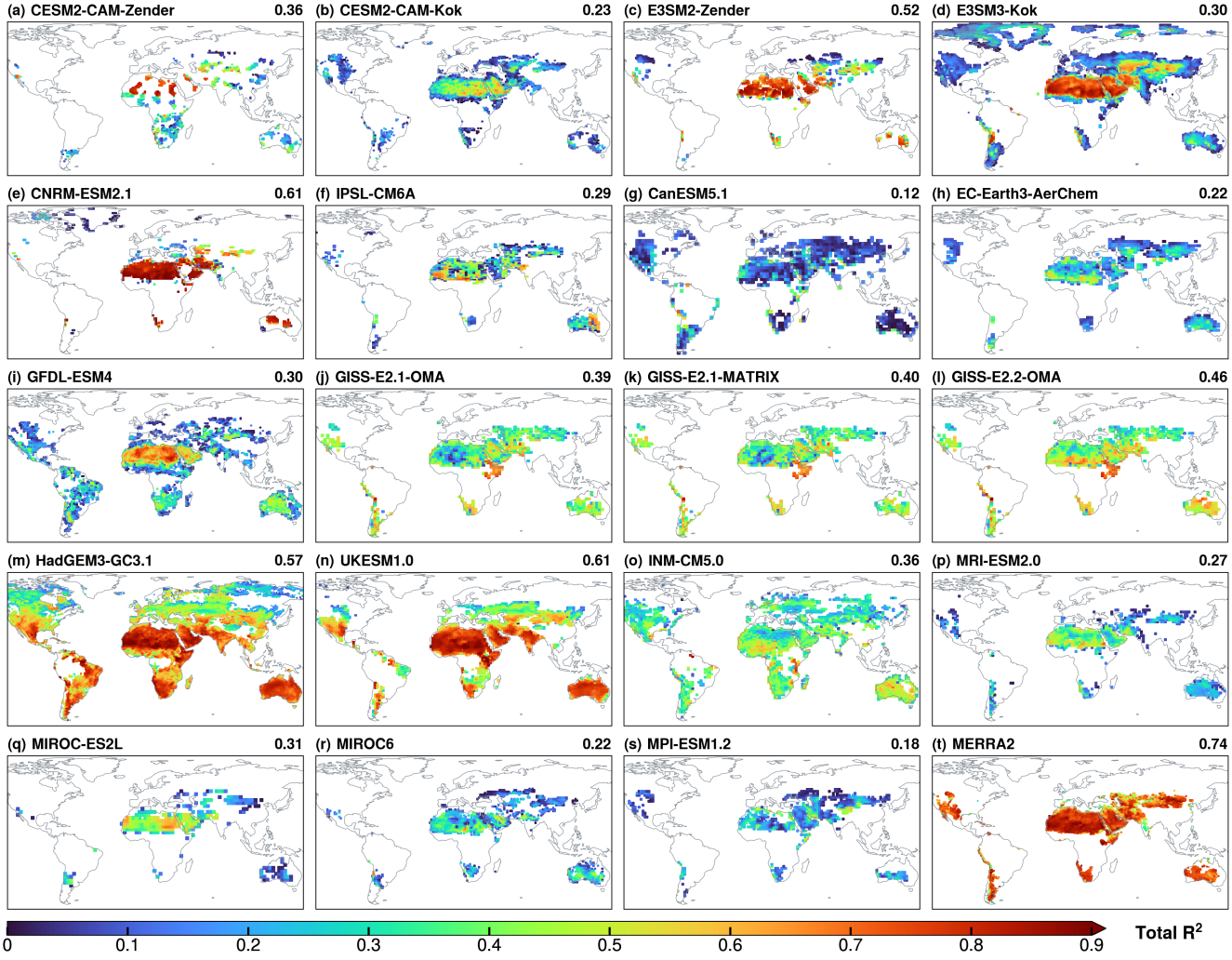

Figure 7. Total explained variance (R^2) in dust emission fluxes by six near-surface predictors (wind speed, precipitation, soil moisture, specific humidity, air temperature and LAI) in Earth system models and MERRA2. Global mean R^2 values are shown on each panel.

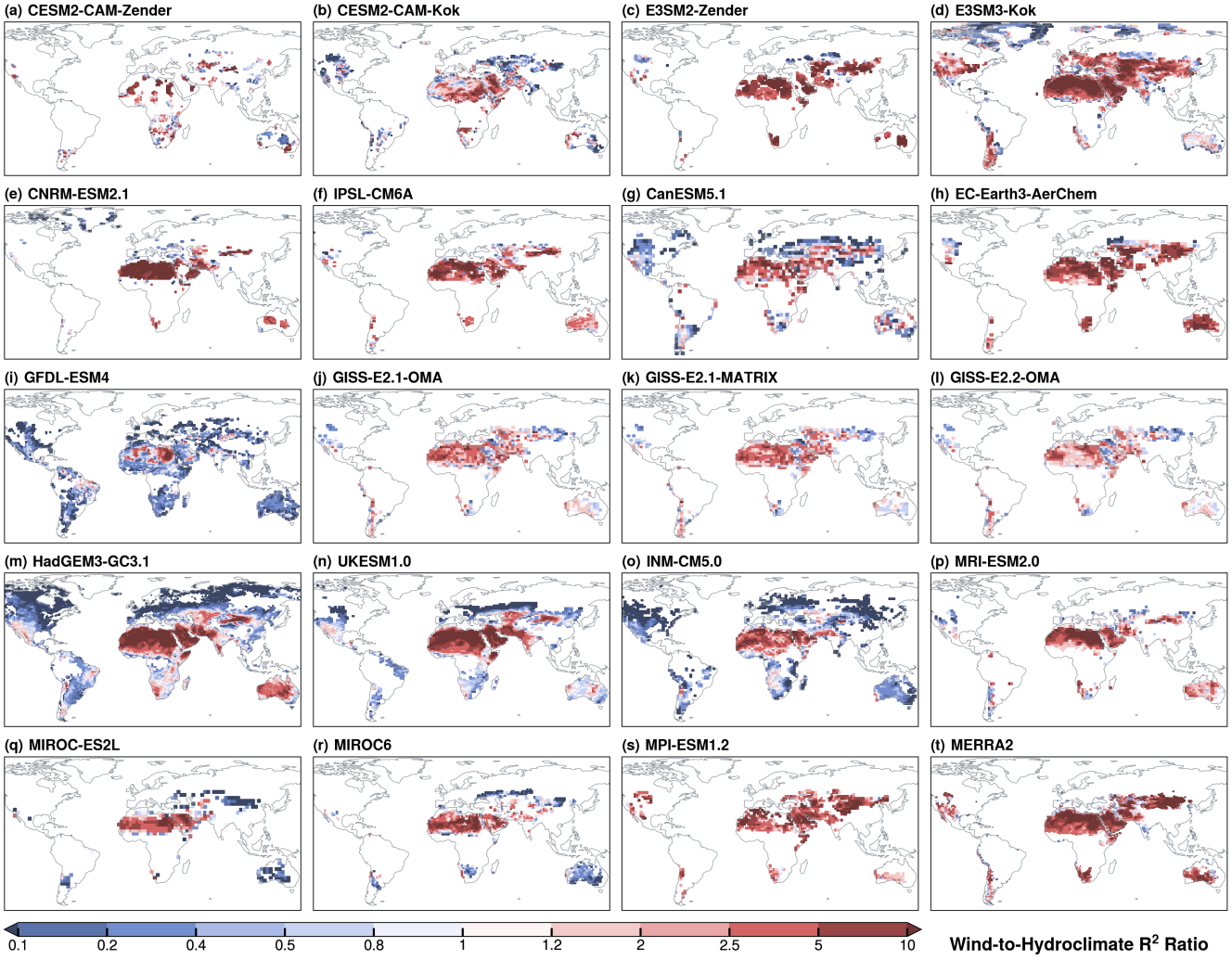

Figure 8. The ratio of wind speed-associated R^2 to the combined R^2 of five hydroclimate variables (precipitation, soil moisture, specific humidity, air temperature and LAI) in Earth system models and MERRA2.

3.3 Relative importance of wind and hydroclimate drivers

In this section, we present the dominance analysis of the collective and relative influence of wind and hydroclimate drivers on the dust emission variability. Figure 7 presents the total variance explained (R^2) by near-surface wind speed and five hydroclimate variables (precipitation, soil moisture, specific humidity, air temperature, and LAI) in the ESMs and MERRA2. Results for CESM2-WACCM-Zender and NorESM2 are very similar to those of CESM2-CAM-Zender and thus not shown.

The ESMs exhibit substantial differences in the total R^2, reflecting a large spread in the internal model variability and coupling strength between dust emission and the six selected predictors. CanESM5.1 yields the lowest global R^2, followed by MPI-ESM1.2, MIROC6, and EC-Earth3-AerChem, in which the selected predictors explain a relatively small fraction of the dust variability. The low explanatory power may be explained by several reasons. Specifically, model deficiencies and errors (e.g., in CanESM5.1, Section 3.1) may weaken or distort the relationships between dust emissions and the predictors. The use of over-simplified parameterizations and/or static land surface input (e.g., in INM-CM5.0) may weaken the dust–predictor relationship. In addition, dust emission involves inherently nonlinear processes and thus its relationship with the predictors may deviate from the linearity assumption in dominance analysis. As shown in Fig. 7, the total R^2 values tend to be much lower in arid and semiarid zones than in the hyperarid zone, likely due to increased nonlinearity between dust emission and hydroclimate variables which diminishes their collective explanatory power in a multilinear regression framework. Finally, the use of monthly model output, due to data availability, may dampen the short-term variability and statistical association between dust emission and the predictors.

Despite these limitations, most ESMs produce significant total R^2 values over major source areas, especially in the hyperarid zone where the total R^2 exceeds 0.6. Switching from the Zender to Kok dust scheme leads to generally lower R^2 values in CESM and E3SM (Fig. 7a–d). The GISS-E2 models show little differences between the OMA or MATRIX schemes, and a modest increase from version 2.1 to 2.2. UKESM1.0 and HadGEM3-GC3.1 show minimal differences, both with high R^2 values globally. MIROC6 yields lower R^2 than MIROC-ES2L, especially over the hyperarid zone. MERRA2 produces higher R^2 than most ESMs, especially over arid and semiarid zones. In summary, there are large spatial variability within individual ESMs and large inter-model discrepancies in the variance explained by the selected predictors.

To assess the relative importance of wind and hydroclimate drivers, Fig. 8 displays the ratio of wind speed-associated R^2 to the combined R^2 of five hydroclimate variables. In all ESMs except GFDL-ESM4, the wind-to-hydroclimate R^2 ratio is well above 1 over the hyperarid zone, which is consistent with the dominant role of wind speed in controlling dust emissions from persistently dry, barren surfaces. In contrast, arid and semiarid zones exhibit greater discrepancies, with ratios either above or below 1 depending on the model. This reflects increased model discrepancies regarding the relative importance of wind and hydroclimate drivers in transitional regions where dust emission is increasingly influenced by hydroclimate and land surface conditions.

Based on the wind-to-hydroclimate R^2 ratios, we classify global dust-emitting areas into three regimes: wind-dominated (ratio$>$1.2), hydroclimate-dominated (ratio$<$0.8), and equally-important (0.8–1.2). We then calculate the fractions of dust emissions originating from the three regimes in each model. The results are displayed in Fig. 9. The ESMs show general

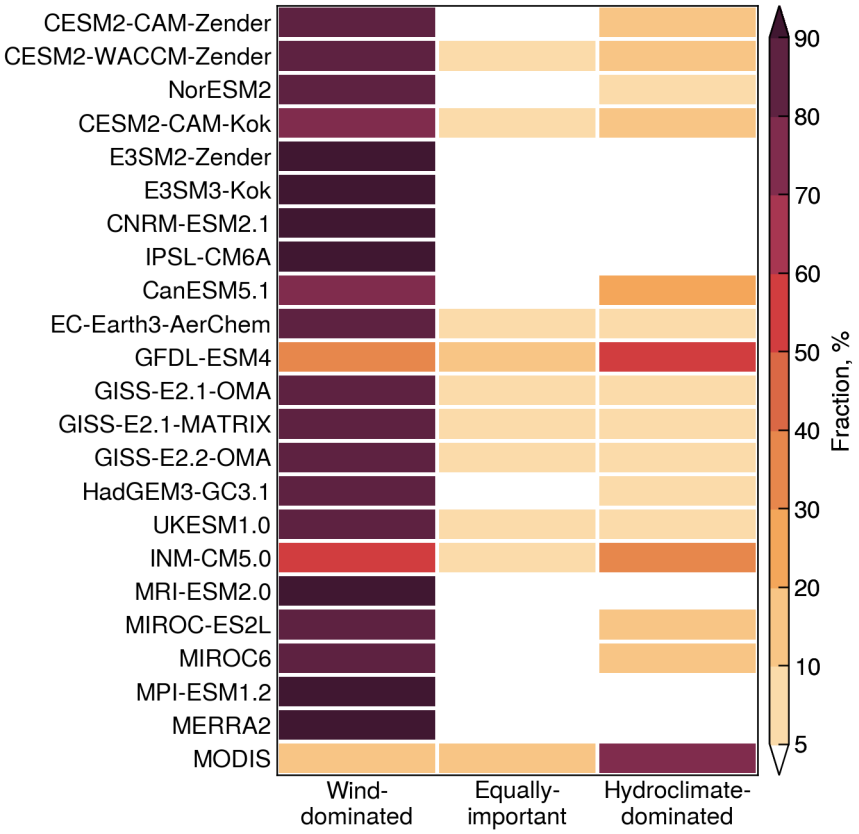

Figure 9. Fractional contributions of wind-dominated, equally-important, and hydroclimate-dominated regimes to global dust emissions in Earth system models and MERRA2.

agreement in the "equally-important" regime, with most models producing less than 10% of dust from regions where wind and hydroclimate drivers have nearly equal influence on dust emissions. GFDL-ESM4 produces the highest contribution (12%) in this regime.

The wind-dominated regime contributes the majority of global dust emissions (>80%) in most ESMs and MERRA2, consistent with the dominant contribution of the hyperarid zone (Fig. 3). However, three models yield anomalously low contributions: GFDL-ESM4 (36%), INM-CM5.0 (54%) and CanESM5.1 (75%). These deviations can be explained by different reasons. As shown in Fig. 3, INM-CM5.0 and CanESM5.1 produce relatively spatially homogeneous emission pattern, which explains the lower contributions from hyperarid or wind-dominated areas. In comparison, the low estimate in GFDL-ESM4 is due to the model's anomalously strong hydroclimate influence over the hyperarid zone. As shown in Fig. 8i, GFDL-ESM4 exhibits markedly low wind-to-hydroclimate ratios (<1) over North Africa, Arabian Peninsula, and Iranian Plateau, which are consequently misclassified into the hydroclimate-dominated regime. These regions are characterized by scarce precipitation and very low hydroclimate variability, which is expected to have negligible influence on dust emissions. For CESM and E3SM, switch-

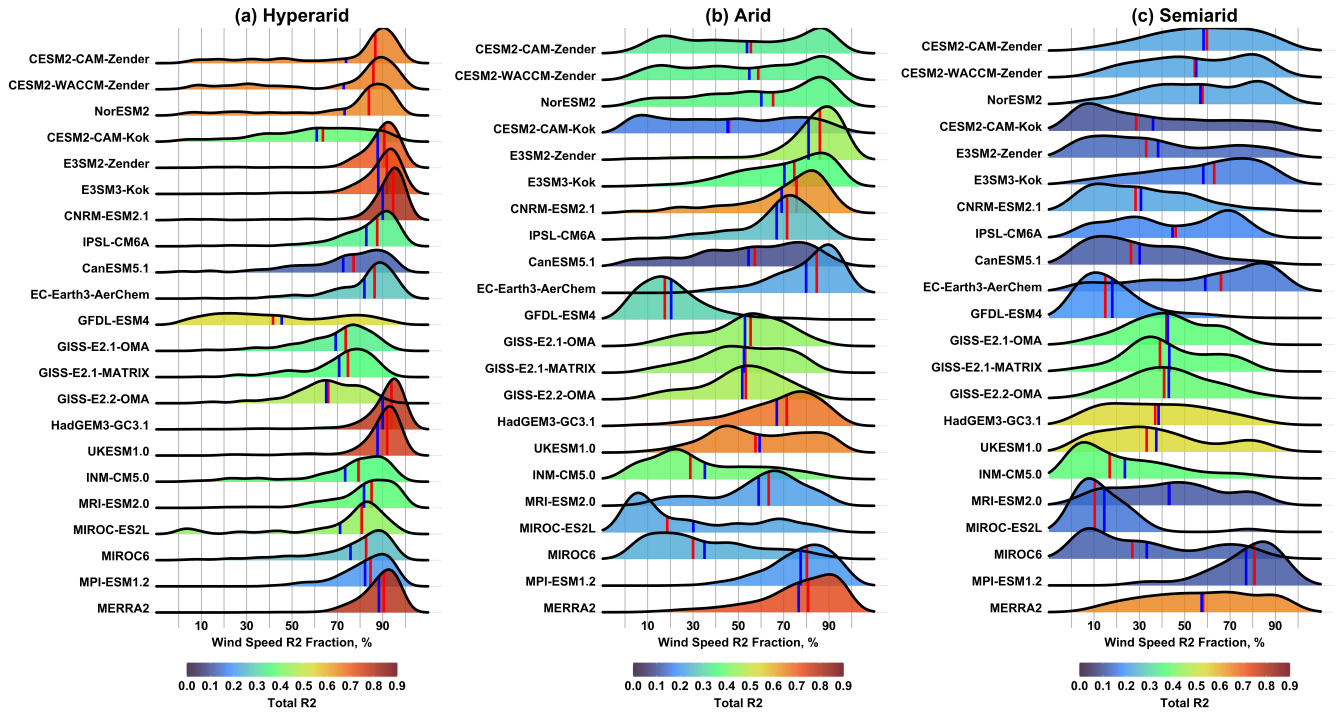

Figure 10. Ridgeline plots of the fractional contributions of wind speed to the total R^2 over (a) hyperarid, (b) arid, and (c) semiarid climate zones. The median and mean values are denoted by red and blue vertical lines, respectively. Color shading represent the mean total R^2 values.

ing from the Zender to Kok dust scheme slightly reduces the wind-dominated dust fraction: from 85% to 80% in CESM, and from 99% to 96% in E3SM. The GISS-E2 models yield similar estimates regardless of model version or aerosol scheme, with 82–85% dust from the wind-dominated regime. Similarly, UKESM1.0 and HadGEM3-GC3.1 yield similar estimates, with 90% of dust emitted from wind-dominated regions. MERRA2 simulates 98% emissions from the wind-dominated regime, higher than most ESMs.

The above analysis not only confirms the anomalous dust emission patterns in CanESM5.1 and INM-CM5.0 as previously shown in Fig. 3, but also identifies GFDL-ESM4 as an outlier due to its misrepresentation of predictor relative importance. Here we further evaluate the contribution of wind speed to the total R^2 in different climate zones. For each climate zone, we use ridgeline plots to illustrate the statistical distributions of grid-level wind speed-associated R^2 fractions. The results are displayed in Fig. 10. In the ridgeline plots, if the median value of wind speed-associated R^2 fractions (denoted by a red vertical line in Fig. 10) is above 50%, it means wind speed dominates the dust variability at more than half of the grid cells. If the median value is below 50%, the dust variability is dominated by hydroclimate drivers at more than half of the grid cells.

In the hyperarid zone (Fig. 10a), most ESMs and MERRA2 capture the dominant control of wind speed, with the median R^2 fractions exceeding 80%. The three GISS-E2 models show similar spatial variability, with slightly lower median values ($\sim$70%). Two models stand out as notable outliers: GFDL-ESM4 and CESM2-CAM-Kok, both of which exhibit large variabil-

ity and low median values. In particular, GFDL-ESM4 yields a median wind R^2 fraction of 42%, indicating an overestimated sensitivity to hydroclimate drivers in the hyperarid zone, particularly over North Africa, Arabian Peninsula and Iranian Plateau (Fig. 8i). Similarly, CESM2-CAM-Kok exhibits large spatial variability with a median wind R^2 fraction of 64%, driven by dominant hydroclimate influence over West Africa and the Tarim Basin (Fig. 8b). In comparison, CESM2-CAM-Zender captures the dominant wind influence with a median value of 86%. The suboptimal performance of CESM2-CAM-Kok relative to CESM2-CAM-Zender persists when comparing common dust-producing areas in the two models.

In the arid zone (Fig. 10b), the total R^2 is generally smaller due to reduced explanatory power of the predictors. The ESMs also show larger disagreement in the relative importance of wind and hydroclimate drivers. The influence of wind speed is reduced and more variable, but still remains dominant in most ESMs and MERRA2. The GISS-E2 models produce relatively equal importance of wind and hydroclimate drivers. In contrast, four models—GFDL-ESM4, INM-CM5.0, MIROC-ES2L and MIROC6—yield dominant hydroclimate influence with the median wind R^2 fraction falling well below 50%, indicating a transition from wind- to hydroclimate-dominated regimes. CESM2-CAM-Kok also reflects this transition, with a median value of 46%. In both CESM and E3SM, switching from the Zender to Kok scheme results in weaker wind and stronger hydroclimate influences, likely due to the physically based soil erodibility treatment in the Kok scheme which enhances the dust sensitivity to hydroclimate variability, as previously suggested in Kok et al. (2014a).

Results for the semiarid zone (Fig. 10c) are considered less robust due to significantly smaller dust-emitting areas or model grid cells (Fig. 1). In general, the wind influence further declines, while hydroclimate divers become more important. The magnitude of this shift, however, varies widely, leading to larger discrepancies. Specifically, hydroclimate drivers continue to dominate in CESM2-CAM-Kok, GFDL-ESM4, INM-CM5.0, MIROC-ES2L and MIROC6, same as in the arid zone. The following ESMs display a clear transition to hydroclimate-dominated regimes: E3SM2-Zender, CNRM-ESM2.1, CanESM5.1, HadGEM3-GC3.1, and UKESM1.0. IPSL-CM6A and GISS-E2 models also show increased hydroclimate influence, though to a lesser extent. The remaining ESMs and MERRA2 continue to display dominance of wind speed, albeit with increased spatial variability.

The above analysis indicates that GFDL-ESM4 and CESM2-CAM-Kok simulate anomalously strong hydroclimate influence in the hyperarid zone. To identify the specific drivers of these anomalies, Fig. 11 presents the median fractional contributions of five hydroclimate variables to the total R^2. In the hyperarid zone, most ESMs capture the negligible sensitivity of dust emission to hydroclimate variables. Several exceptions exist, however. CESM2-CAM-Kok shows unusually strong influence from precipitation and specific humidity, while GFDL-ESM4 exhibits anomalously strong sensitivity to soil moisture. The GISS-E2 models display moderately elevated sensitivity to soil moisture and specific humidity, which explains their moderate wind influence in the hyperarid zone (Fig. 10a).

The overestimation of hydroclimate influence in the hyperarid zone may be explained by a combination of two mechanisms: (1) the hydroclimate variability is overestimated in the model, which induces spurious effects on dust emissions; or (2) the hydroclimate variability is reasonably captured, but the dust scheme incorporates overly strong sensitivity to hydroclimate drivers. Shevliakova et al. (2024) reported that the GFDL-ESM4 land model significantly overestimates soil moisture over dryland regions, with values more than double those from satellite observations in dust source regions like the central Sahara

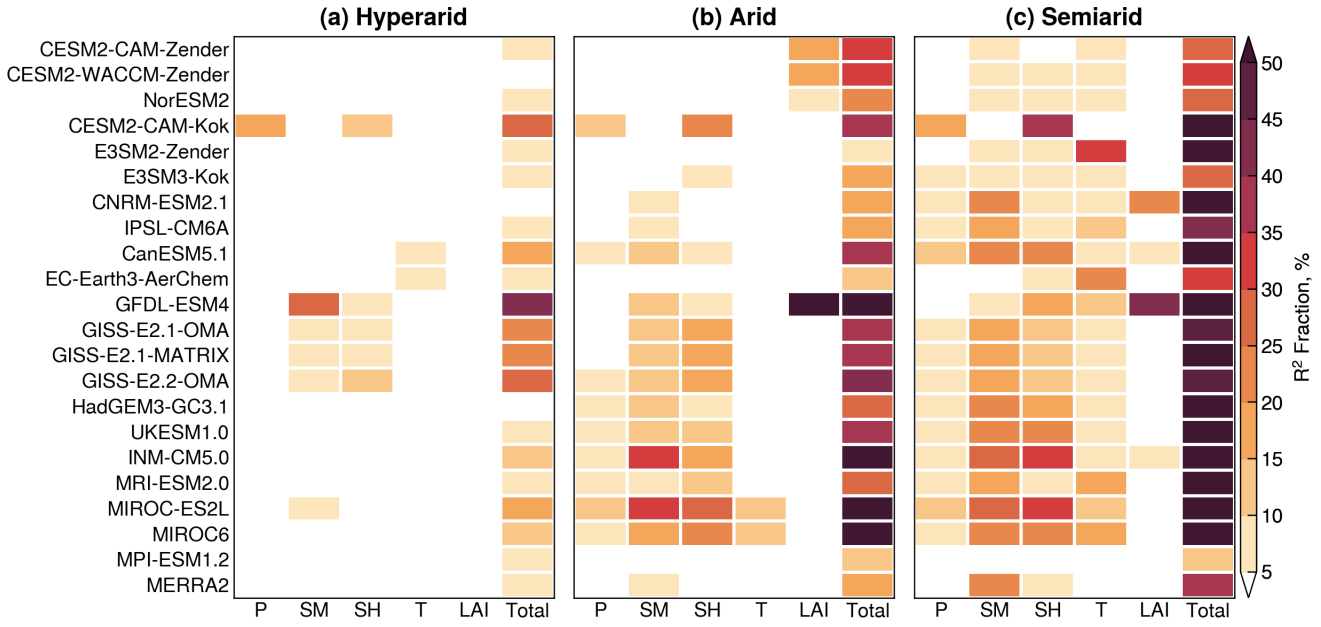

Figure 11. Median factional contributions of hydroclimate variables to the total explained variance (R^2) in Earth system models and MERRA2 over (a) hyperarid, (b) arid, and (c) semiarid climate zones. Hydroclimate variables are precipitation (P), soil moisture (SM), specific humidity (SH), air temperature (T), and leaf area index (LAI).

and Tarim Basin. This bias likely explains the strong apparent sensitivity of dust emission to soil moisture in GFDL-ESM4 (Fig. 11a).

The abnormal hydroclimate influence in CESM2-CAM-Kok may be partly explained by dust emission parameterizations in the Kok scheme, which introduces enhanced sensitivity to the threshold wind velocity compared to the Zender scheme (Kok et al., 2014a). Because of this heightened dependence on land surface conditions, the Kok scheme does not require predefined dust source functions and is considered more physically realistic for projecting dust responses to future climate and land-use changes. Another possible reason is the relatively short simulation period in CESM2-CAM-Kok (2004–2013), which may not fully capture the long-term variability and predictor influence as in CESM2-CAM-Zender (1980–2014). In this regard, the E3SM experiments provide a more robust comparison between the Zender and Kok schemes. As shown in Fig. 11a, the E3SM models exhibit negligible hydroclimate influence in the hyperarid zone, regardless of the dust scheme used. In the arid zone, however, E3SM3-Kok shows higher hydroclimate influence than E3SM2-Zender due to increased sensitivity to specific humidity (Fig. 11b). This comparison provides additional evidence that the Kok scheme amplifies the dust emission sensitivity to hydroclimate conditions.

In the arid zone (Fig. 11b), most ESMs show enhanced influence from soil moisture and specific humidity, consistent with empirical evidence that both variables strongly affect the soil erodibility and wind erosion risk (e.g., Csavina et al., 2014; RAVI et al., 2006; Kim and Choi, 2015). Interpreting the LAI influence, however, is more complex due to several factors. First, unlike

other hydroclimate variables, LAI can be either prescribed from climatology or simulated by the model's dynamic vegetation component (Table 1). Models using prescribed LAI are expected to show minimal interannual variability and hence limited influence on dust emissions. Second, the LAI effect on dust emission is treated differently. For example, CESM assumes a linear relationship between bare soil fraction and LAI when LAI is below 0.3, while GFDL-ESM4 assumes an exponential decrease in bare soil fraction as a function of LAI. Because LAI is often used to derive bare soil fraction in vertical dust flux calculations, these differences can alter the modeled dust sensitivity to vegetation cover. Most ESMs in Fig. 11b exhibit weak to negligible LAI influence, likely reflecting either prescribed LAI or the normalization of dust fluxes prior to dominance analysis (see Section 2). One outlier is GFDL-ESM4 which exhibits the strongest sensitivity to LAI, even well above the sensitivity to soil moisture. This can be explained by the strong coupled between LAI and dust emission in the model, and the fact that no normalization was applied to GFDL-ESM4 due to missing bare soil fraction output from the CMIP6 archive.

4 Conclusions

This study evaluates discrepancies and biases among 21 ESMs in representing the interannual variability of windblown dust emissions and the relative importance of near-surface wind speed and hydroclimate drivers (precipitation, soil moisture, specific humidity, air temperature, and LAI). We treat dust emission flux as an unobservable, model-specific quantity and use dominance analysis to quantify the variance explained in dust emission fluxes by wind and hydroclimate drivers within each model. The analysis is conducted over three climatologically defined climate zones (hyperarid, arid, and semiarid), and further examines the effect of dust emission parameterizations through paired CESM and E3SM experiments with the Zender et al. (2003) and Kok et al. (2014b) schemes.

The hyperarid zone contributes more than half of global dust emissions in all models except CanESM5.1 and INM-CM5.0, which simulate relatively spatially even emission patterns with less than 50% from the hyperarid zone, likely due to known deficiencies and over-simplifications in dust emission representations. In the hyperarid zone, the ESMs exhibit poor agreement with each other and with MERRA2 in simulating the dust variability, with only 10% of pairwise model comparisons yielding statistically significant, positive correlations. In arid and semiarid zones, the ESMs exhibit a dipole pattern with both improved agreement and increased disagreement. This behavior can be explained by a "double-edged sword" effect of land surface memory: models with coherent representations of hydroclimate variability converge in their dust variability, while those with divergent hydroclimate representations diverge in dust emission responses.

The relative influence of wind and hydroclimate drivers also varies with climate regimes. Most ESMs capture the dominant control of wind speed and weak sensitivity to hydroclimate conditions in the hyperarid zone, except CESM2-CAM-Kok and GFDL-ESM4, both of which show great spatial variability and abnormally strong influence from precipitation, specific humidity, and soil moisture. The overestimated hydroclimate influence in GFDL-ESM4 can be explained by the model's overestimation of soil moisture and consequent spurious effects on dust emissions. The enhanced hydroclimate influence in CESM2-CAM-Kok (relative to CESM2-CAM-Zender) may be explained, at least partly, by the physically based soil erodibility formulations in the Kok et al. (2014b) scheme, which replaces the use of predefined dust source functions. A similar pattern

is found in E3SM, where switching from the Zender et al. (2003) to the Kok et al. (2014b) scheme strengthens the hydroclimate influence in the arid zone. However, due to concurrent updates in model physics (e.g., dust mineralogy, radiative feedbacks, and meteorology), further experiments are needed to isolate the effects of dust emission parameterizations on dust–climate sensitivities.

In arid and semiarid zones, the influence of wind speed generally weakens while the hydroclimate influence strengthens. However, the relative importance of wind and hydroclimate drivers becomes increasingly inconsistent between the models, with an increasing number of ESMs shifting toward comparable or dominant-dominated regimes. In general, MERRA2 produces stronger wind influence and weaker hydroclimate influence than the ESMs.

In summary, this study provides new insights into how ESMs represent the temporal variability and physical drivers of windblown dust emissions. Most ESMs capture the dominant wind control over permanently dry, barren surfaces, their poor agreement in dust variability highlights large inconsistencies in the simulated near-surface winds. The dipole model behavior in arid and semiarid zones underscores the important role of hydroclimate variability and land surface processes. Improving model representations of soil and vegetation dynamics and dust-climate interactions in these regions is essential for reducing uncertainties in future projections of dust emissions under changing climate and land-use conditions.

Data availability. Model comparison and dominance analysis results are available at https://doi.org/10.5281/zenodo.15741734.

Author contributions. XX designed this study with input from LL. XX and XL performed the analysis and wrote the initial manuscript. LL performed CESM2-CAM-Kok simulations. YF performed E3SM simulations. All authors edited the manuscript.

Competing interests. The authors declare no competing interests.

Acknowledgements. X.L. and X.X. are partially supported by the NASA Land-Cover and Land-Use Change Program. Y.F. acknowledges the support of the Energy Exascale Earth System Model (E3SM) project, funded by the U.S. Department of Energy (DOE), Office of Science, Office of Biological and Environmental Research. The work at Argonne National Laboratory was supported by the U.S. DOE Office of Science under contract DE-AC02-06CH11357. L.L. acknowledges support from the U.S. Department of Energy (DOE) under award DE-SC0021302, and from the Earth Surface Mineral Dust Source Investigation (EMIT), a National Aeronautics and Space Administration (NASA) Earth Ventures-Instrument (EVI-4) mission. He also acknowledges the high-performance computing resources provided by Derecho at the National Center for Atmospheric Research (NCAR), through NCAR's Computational and Information Systems Laboratory (CISL), which is sponsored by the National Science Foundation (NSF). The authors acknowledge the World Climate Research Programme for coordinating and promoting CMIP6, and thank the climate modeling groups for producing and making available their model output, the

Earth System Grid Federation (ESGF) for archiving the data and providing access, and the multiple funding agencies who support CMIP6 and ESGF.

References

Albani, S., Mahowald, N. M., Perry, A. T., Scanza, R. A., Zender, C. S., Heavens, N. G., Maggi, V., Kok, J. F., and Otto-Bliesner, B. L.: Improved dust representation in the Community Atmosphere Model, Journal of Advances in Modeling Earth Systems, 6, 541–570, https://doi.org/10.1002/2013MS000279, 2015.

Aryal, Y. and Evans, S.: Dust emission response to precipitation and temperature anomalies under different climatic conditions, Science of the Total Environment, 874, https://doi.org/10.1016/j.scitotenv.2023.162335, 2023.

Aryal, Y. N. and Evans, S.: Global Dust Variability Explained by Drought Sensitivity in CMIP6 Models, Journal of Geophysical Research: Earth Surface, 126, https://doi.org/10.1029/2021JF006073, 2021.

Azen, R. and Budescu, D. V.: The Dominance Analysis Approach for Comparing Predictors in Multiple Regression, Psychological Methods, 8, 129–148, https://doi.org/10.1037/1082-989X.8.2.129, 2003.

Balkanski, Y., Schulz, M., Claquin, T., Moulin, C., and Ginoux, P.: Global Emissions of Mineral Aerosol: Formulation and Validation using Satellite Imagery, in: Emissions of Atmospheric Trace Compounds, edited by Granier, C., Artaxo, P., and Reeves, C. E., pp. 239–267, Springer, https://doi.org/10.1007/978-1-4020-2167-1_6, 2004.

Bauer, S. E., Tsigaridis, K., Faluvegi, G., Nazarenko, L., Miller, R. L., Kelley, M., and Schmidt, G.: The Turning Point of the Aerosol Era, Journal of Advances in Modeling Earth Systems, 14, https://doi.org/10.1029/2022MS003070, 2022.

Bergametti, G., Marticorena, B., Rajot, J. L., Chatenet, B., Féron, A., Gaimoz, C., Siour, G., Coulibaly, M., Koné, I., Maman, A., and Zakou, A.: Dust Uplift Potential in the Central Sahel: An Analysis Based on 10 years of Meteorological Measurements at High Temporal Resolution, Journal of Geophysical Research: Atmospheres, 122, 433–12, https://doi.org/10.1002/2017JD027471, 2017.

Bryant, R. G.: Recent advances in our understanding of dust source emission processes, Progress in Physical Geography, 37, 397–421, https://doi.org/10.1177/0309133313479391, 2013.

Budescu, D. V.: Dominance analysis: A new approach to the problem of relative importance of predictors in multiple regression, Psychological Bulletin, 114, 542–551, https://doi.org/10.1037/0033-2909.114.3.542, 1993.

Bullard, J. E., Harrison, S. P., Baddock, M. C., Drake, N., Gill, T. E., McTainsh, G., and Sun, Y.: Preferential dust sources: A geomorphological classification designed for use in global dust-cycle models, Journal of Geophysical Research: Earth Surface, 116, https://doi.org/10.1029/2011JF002061, 2011.

Cakmur, R. V., Miller, R. L., and Torres, O.: Incorporating the effect of small-scale circulations upon dust emission in an atmospheric general circulation model, Journal of Geophysical Research: Atmospheres, 109, https://doi.org/10.1029/2003jd004067, 2004.

Cheng, T., Peng, Y., Feichter, J., and Tegen, I.: An improvement on the dust emission scheme in the global aerosol-climate model ECHAM5-HAM, Atmospheric Chemistry and Physics, 8, 1105–1117, https://doi.org/10.5194/acp-8-1105-2008, 2008.

Cowie, S. M., Marsham, J. H., and Knippertz, P.: The importance of rare, high-wind events for dust uplift in northern Africa, Geophysical Research Letters, 42, 8208–8215, https://doi.org/10.1002/2015GL065819, 2015.

Csavina, J., Field, J., Félix, O., Corral-Avitia, A. Y., Sáez, A. E., and Betterton, E. A.: Effect of wind speed and relative humidity on atmospheric dust concentrations in semi-arid climates, Science of the Total Environment, 487, 82–90, https://doi.org/10.1016/j.scitotenv.2014.03.138, 2014.

Engelstaedter, S., Kohfeld, K. E., Tegen, I., and Harrison, S. P.: Controls of dust emissions by vegetation and topographic depressions: An evaluation using dust storm frequency data, Geophysical Research Letters, 30, https://doi.org/10.1029/2002GL016471, 2003.

Evan, A. T.: Surface Winds and Dust Biases in Climate Models, Geophysical Research Letters, 45, 1079–1085, https://doi.org/10.1002/2017GL076353, 2018.

Evan, A. T., Flamant, C., Fiedler, S., and Doherty, O.: An analysis of aeolian dust in climate models, Geophysical Research Letters, 41, 5996–6001, https://doi.org/10.1002/2014GL060545, 2014.

Evans, S., Ginoux, P., Malyshev, S., and Shevliakova, E.: Climate-vegetation interaction and amplification of Australian dust variability, Geophysical Research Letters, 43, 823–11, https://doi.org/10.1002/2016GL071016, 2016.

Fécan, F., Marticorena, B., and Bergametti, G.: Parametrization of the increase of the aeolian erosion threshold wind friction velocity due to soil moisture for arid and semi-arid areas, Annales Geophysicae, 17, 149, https://doi.org/10.1007/s005850050744, 1999.

Feng, Y., Wang, H., Rasch, P. J., Zhang, K., Lin, W., Tang, Q., Xie, S., Hamilton, D. S., Mahowald, N., and Yu, H.: Global Dust Cycle and Direct Radiative Effect in E3SM Version 1: Impact of Increasing Model Resolution, Journal of Advances in Modeling Earth Systems, https://doi.org/10.1029/2021MS002909, 2022.

Gelaro, R., McCarty, W., Suárez, M. J., Todling, R., Molod, A., Takacs, L., Randles, C. A., Darmenov, A., Bosilovich, M. G., Reichle, R., Wargan, K., Coy, L., Cullather, R., Draper, C., Akella, S., Buchard, V., Conaty, A., da Silva, A. M., Gu, W., Kim, G. K., Koster, R., Lucchesi, R., Merkova, D., Nielsen, J. E., Partyka, G., Pawson, S., Putman, W., Rienecker, M., Schubert, S. D., Sienkiewicz, M., and Zhao, B.: The modern-era retrospective analysis for research and applications, version 2 (MERRA-2), Journal of Climate, 30, 5419–5454, https://doi.org/10.1175/JCLI-D-16-0758.1, 2017.

Gettelman, A., Mills, M. J., Kinnison, D. E., Garcia, R. R., Smith, A. K., Marsh, D. R., Tilmes, S., Vitt, F., Bardeen, C. G., McInerny, J., Liu, H. L., Solomon, S. C., Polvani, L. M., Emmons, L. K., Lamarque, J. F., Richter, J. H., Glanville, A. S., Bacmeister, J. T., Phillips, A. S., Neale, R. B., Simpson, I. R., DuVivier, A. K., Hodzic, A., and Randel, W. J.: The Whole Atmosphere Community Climate Model Version 6 (WACCM6), Journal of Geophysical Research: Atmospheres, 124, 12 380–12 403, https://doi.org/10.1029/2019JD030943, 2019.

Ginoux, P., Chin, M., Tegen, I., Prospero, J. M., Holben, B., Dubovik, O., and Lin, S. J.: Sources and distributions of dust aerosols simulated with the GOCART model, Journal of Geophysical Research Atmospheres, 106, 20 255–20 273, https://doi.org/10.1029/2000JD000053, 2001.

Ginoux, P., Prospero, J. M., Gill, T. E., Hsu, N. C., and Zhao, M.: Global-scale attribution of anthropogenic and natural dust sources and their emission rates based on MODIS Deep Blue aerosol products, Reviews of Geophysics, 50, https://doi.org/10.1029/2012RG000388, 2012.

Gliß, J., Mortier, A., Schulz, M., Andrews, E., Balkanski, Y., Bauer, S. E., Benedictow, A. M., Bian, H., Checa-Garcia, R., Chin, M., Ginoux, P., Griesfeller, J. J., Heckel, A., Kipling, Z., Kirkeväg, A., Kokkola, H., Laj, P., Le Sager, P., Tronstad Lund, M., Lund Myhre, C., Matsui, H., Myhre, G., Neubauer, D., Van Noije, T., North, P., Olivié, D. J., Rémy, S., Sogacheva, L., Takemura, T., Tsigaridis, K., and Tsyro, S. G.: AeroCom phase III multi-model evaluation of the aerosol life cycle and optical properties using ground- And space-based remote sensing as well as surface in situ observations, Atmospheric Chemistry and Physics, 21, 87–128, https://doi.org/10.5194/acp-21-87-2021, 2021.

Grini, A., Myhre, G., Zender, C. S., and Isaksen, I. S.: Model simulations of dust sources and transport in the global atmosphere: Effects of soil erodibility and wind speed variability, Journal of Geophysical Research D: Atmospheres, 110, 1–14, https://doi.org/10.1029/2004JD005037, 2005.

Hajima, T., Watanabe, M., Yamamoto, A., Tatebe, H., Noguchi, M. A., Abe, M., Ohgaito, R., Ito, A., Yamazaki, D., Okajima, H., Ito, A., Takata, K., Ogochi, K., Watanabe, S., and Kawamiya, M.: Development of the MIROC-ES2L Earth system model and the evaluation of biogeochemical processes and feedbacks, Geoscientific Model Development, 13, 2197–2244, https://doi.org/10.5194/gmd-13-2197-2020, 2020.

Huneeus, N., Schulz, M., Balkanski, Y., Griesfeller, J., Prospero, J., Kinne, S., Bauer, S., Boucher, O., Chin, M., Dentener, F., Diehl, T., Easter, R., Fillmore, D., Ghan, S., Ginoux, P., Grini, A., Horowitz, L., Koch, D., Krol, M. C., Landing, W., Liu, X., Mahowald, N., Miller, R., Morcrette, J. J., Myhre, G., Penner, J., Perlwitz, J., Stier, P., Takemura, T., and Zender, C. S.: Global dust model intercomparison in AeroCom phase i, Atmospheric Chemistry and Physics, 11, 7781–7816, https://doi.org/10.5194/acp-11-7781-2011, 2011.

Kim, D., Chin, M., Yu, H., Diehl, T., Tan, Q., Kahn, R. A., Tsigaridis, K., Bauer, S. E., Takemura, T., Pozzoli, L., Bellouin, N., Schulz, M., Peyridieu, S., Chédin, A., and Koffi, B.: Sources, sinks, and transatlantic transport of North African dust aerosol: A multimodel analysis and comparison with remote sensing data, Journal of Geophysical Research, 119, 6259–6277, https://doi.org/10.1002/2013JD021099, 2014.

Kim, D., Chin, M., Schuster, G., Yu, H., Takemura, T., Tuccella, P., Ginoux, P., Liu, X., Shi, Y., Matsui, H., Tsigaridis, K., Bauer, S. E., Kok, J. F., and Schulz, M.: Where Dust Comes From: Global Assessment of Dust Source Attributions With AeroCom Models, Journal of Geophysical Research: Atmospheres, 129, e2024JD041 377, https://doi.org/https://doi.org/10.1029/2024JD041377, 2024.

Kim, H. and Choi, M.: Impact of soil moisture on dust outbreaks in East Asia: Using satellite and assimilation data, Geophysical Research Letters, 42, 2789–2796, https://doi.org/https://doi.org/10.1002/2015GL063325, 2015.

Knippertz, P. and Todd, M. C.: Mineral dust aerosols over the Sahara: Meteorological controls on emission and transport and implications for modeling, Reviews of Geophysics, 50, https://doi.org/10.1029/2011RG000362, 2012.

Kok, J. F., Albani, S., Mahowald, N. M., and Ward, D. S.: An improved dust emission model - Part 2: Evaluation in the Community Earth System Model, with implications for the use of dust source functions, Atmospheric Chemistry and Physics, 14, 13 043–13 061, https://doi.org/10.5194/acp-14-13043-2014, 2014a.

Kok, J. F., Mahowald, N. M., Fratini, G., Gillies, J. A., Ishizuka, M., Leys, J. F., Mikami, M., Park, M. S., Park, S. U., Van Pelt, R. S., and Zobeck, T. M.: An improved dust emission model - Part 1: Model description and comparison against measurements, Atmospheric Chemistry and Physics, 14, 13 023–13 041, https://doi.org/10.5194/acp-14-13023-2014, 2014b.

Kok, J. F., Storelvmo, T., Karydis, V. A., Adebiyi, A. A., Mahowald, N. M., Evan, A. T., He, C., and Leung, D. M.: Mineral dust aerosol impacts on global climate and climate change, Nature Reviews Earth and Environment, 4, 71–86, https://doi.org/10.1038/s43017-022-00379-5, 2023.

Koster, R. D., Guo, Z., Yang, R., Dirmeyer, P. A., Mitchell, K., and Puma, M. J.: On the nature of soil moisture in land surface models, Journal of Climate, 22, 4322–4335, https://doi.org/10.1175/2009JCLI2832.1, 2009.

Leung, D. M., Kok, J. F., Li, L., Lawrence, D. M., Mahowald, N. M., Tilmes, S., and Kluzek, E.: A global dust emission dataset for estimating dust radiative forcings in climate models, Atmos. Chem. Phys., 25, 2311–2331, https://doi.org/10.5194/acp-25-2311-2025, 2025.

Li, L., Mahowald, N. M., Kok, J. F., Liu, X., Wu, M., Leung, D. M., Hamilton, D. S., Emmons, L. K., Huang, Y., Sexton, N., Meng, J., and Wan, J.: Importance of different parameterization changes for the updated dust cycle modeling in the Community Atmosphere Model (version 6.1), Geoscientific Model Development, 15, 8181–8219, https://doi.org/10.5194/gmd-15-8181-2022, 2022.

Li, L., Mahowald, N. M., Gonçalves Ageitos, M., Obiso, V., Miller, R. L., Pérez García-Pando, C., Di Biagio, C., Formenti, P., Brodrick, P. G., Clark, R. N., Green, R. O., Kokaly, R., Swayze, G., and Thompson, D. R.: Improved constraints on hematite refractive index for estimating climatic effects of dust aerosols, Communications Earth & Environment, 5, 295, https://doi.org/10.1038/s43247-024-01441-4, 2024.

Lurton, T., Balkanski, Y., Bastrikov, V., Bekki, S., Bopp, L., Braconnot, P., Brockmann, P., Cadule, P., Contoux, C., Cozic, A., Cugnet, D., Dufresne, J.-L., Éthé, C., Foujols, M.-A., Ghattas, J., Hauglustaine, D., Hu, R.-M., Kageyama, M., Khodri, M., Lebas, N., Levavasseur, G., Marchand, M., Ottlé, C., Peylin, P., Sima, A., Szopa, S., Thiéblemont, R., Vuichard, N., and Boucher, O.: Implementation

of the CMIP6 Forcing Data in the IPSL-CM6A-LR Model, Journal of Advances in Modeling Earth Systems, 12, e2019MS001 940, https://doi.org/https://doi.org/10.1029/2019MS001940, 2020.

Marticorena, B. and Bergametti, G.: Modeling the atmospheric dust cycle: 1. Design of a soil-derived dust emission scheme, Journal of Geophysical Research, 100, https://doi.org/10.1029/95jd00690, 1995.

Mauritsen, T., Bader, J., Becker, T., Behrens, J., Bittner, M., Brokopf, R., Brovkin, V., Claussen, M., Crueger, T., Esch, M., Fast, I., Fiedler, S., Fläschner, D., Gayler, V., Giorgetta, M., Goll, D. S., Haak, H., Hagemann, S., Hedemann, C., Hohenegger, C., Ilyina, T., Jahns, T., Jimenéz-de-la Cuesta, D., Jungclaus, J., Kleinen, T., Kloster, S., Kracher, D., Kinne, S., Kleberg, D., Lasslop, G., Kornblueh, L., Marotzke, J., Matei, D., Meraner, K., Mikolajewicz, U., Modali, K., Möbis, B., Müller, W. A., Nabel, J. E. M. S., Nam, C. C. W., Notz, D., Nyawira, S.-S., Paulsen, H., Peters, K., Pincus, R., Pohlmann, H., Pongratz, J., Popp, M., Raddatz, T. J., Rast, S., Redler, R., Reick, C. H., Rohrschneider, T., Schemann, V., Schmidt, H., Schnur, R., Schulzweida, U., Six, K. D., Stein, L., Stemmler, I., Stevens, B., von Storch, J.-S., Tian, F., Voigt, A., Vrese, P., Wieners, K.-H., Wilkenskjeld, S., Winkler, A., and Roeckner, E.: Developments in the MPI-M Earth System Model version 1.2 (MPI-ESM1.2) and Its Response to Increasing CO2, Journal of Advances in Modeling Earth Systems, 11, 998–1038, https://doi.org/https://doi.org/10.1029/2018MS001400, 2019.

Miller, R. L., Cakmur, R. V., Perlwitz, J., Geogdzhayev, I. V., Ginoux, P., Koch, D., Kohfeld, K. E., Prigent, C., Ruedy, R., Schmidt, G. A., and Tegen, I.: Mineral dust aerosols in the NASA Goddard Institute for Space Sciences ModelE atmospheric general circulation model, Journal of Geophysical Research Atmospheres, 111, https://doi.org/10.1029/2005JD005796, 2006.

Miller, R. L., Schmidt, G. A., Nazarenko, L. S., Bauer, S. E., Kelley, M., Ruedy, R., Russell, G. L., Ackerman, A. S., Aleinov, I., Bauer, M., Bleck, R., Canuto, V., Cesana, G., Cheng, Y., Clune, T. L., Cook, B. I., Cruz, C. A., Del Genio, A. D., Elsaesser, G. S., Faluvegi, G., Kiang, N. Y., Kim, D., Lacis, A. A., Leboissetier, A., LeGrande, A. N., Lo, K. K., Marshall, J., Matthews, E. E., McDermid, S., Mezuman, K., Murray, L. T., Oinas, V., Orbe, C., Pérez García-Pando, C., Perlwitz, J. P., Puma, M. J., Rind, D., Romanou, A., Shindell, D. T., Sun, S., Tausnev, N., Tsigaridis, K., Tselioudis, G., Weng, E., Wu, J., and Yao, M. S.: CMIP6 Historical Simulations (1850–2014) With GISS-E2.1, Journal of Advances in Modeling Earth Systems, 13, https://doi.org/10.1029/2019MS002034, 2021.

Nandintsetseg, B. and Shinoda, M.: Land surface memory effects on dust emission in a Mongolian temperate grassland, Journal of Geophysical Research: Biogeosciences, 120, 414–427, https://doi.org/10.1002/2014JG002708, 2015.

Peng, Y., Von Salzen, K., and Li, J.: Simulation of mineral dust aerosol with Piecewise Log-normal Approximation (PLA) in CanAM4-PAM, Atmospheric Chemistry and Physics, 12, 6891–6914, https://doi.org/10.5194/acp-12-6891-2012, 2012.

Prospero, J. M. and Lamb, P. J.: African Droughts and Dust Transport to the Caribbean: Climate Change Implications, Science, 302, 1024–1027, https://doi.org/10.1126/science.1089915, 2003.

Prospero, J. M., Ginoux, P., Torres, O., Nicholson, S. E., and Gill, T. E.: Environmental characterization of global sources of atmospheric soil dust identified with the Nimbus 7 Total Ozone Mapping Spectrometer (TOMS) absorbing aerosol product, Reviews of Geophysics, 40, 2–1, https://doi.org/10.1029/2000RG000095, 2002.

Pu, B. and Ginoux, P.: The impact of the Pacific Decadal Oscillation on springtime dust activity in Syria, Atmospheric Chemistry and Physics, 16, 13 431–13 448, https://doi.org/10.5194/acp-16-13431-2016, 2016.

Pu, B. and Ginoux, P.: How reliable are CMIP5 models in simulating dust optical depth?, Atmospheric Chemistry and Physics, 18, 12 491–12 510, https://doi.org/10.5194/acp-18-12491-2018, 2018.

Randles, C. A., da Silva, A. M., Buchard, V., Colarco, P. R., Darmenov, A., Govindaraju, R., Smirnov, A., Holben, B., Ferrare, R., Hair, J., Shinozuka, Y., and Flynn, C. J.: The MERRA-2 aerosol reanalysis, 1980 onward. Part I: System description and data assimilation evaluation, Journal of Climate, 30, 6823–6850, https://doi.org/10.1175/JCLI-D-16-0609.1, 2017.

RAVI, S., ZOBECK, T. E. D. M., OVER, T. M., OKIN, G. S., and D'ODORICO, P.: On the effect of moisture bonding forces in air-dry soils on threshold friction velocity of wind erosion, Sedimentology, 53, 597–609, https://doi.org/https://doi.org/10.1111/j.1365-3091.2006.00775.x, 2006.

Ridley, D. A., Heald, C. L., Pierce, J. R., and Evans, M. J.: Toward resolution-independent dust emissions in global models: Impacts on the seasonal and spatial distribution of dust, Geophysical Research Letters, 40, 2873–2877, https://doi.org/10.1002/grl.50409, 2013.

Rind, D., Orbe, C., Jonas, J., Nazarenko, L., Zhou, T., Kelley, M., Lacis, A., Shindell, D., Faluvegi, G., Romanou, A., Russell, G., Tausnev, N., Bauer, M., and Schmidt, G.: GISS Model E2.2: A Climate Model Optimized for the Middle Atmosphere—Model Structure, Climatology, Variability, and Climate Sensitivity, Journal of Geophysical Research: Atmospheres, 125, https://doi.org/10.1029/2019JD032204, 2020.

Roberts, M. J., Baker, A., Blockley, E. W., Calvert, D., Coward, A., Hewitt, H. T., Jackson, L. C., Kuhlbrodt, T., Mathiot, P., Roberts, C. D., Schiemann, R., Seddon, J., Vannière, B., and Vidale, P. L.: Description of the resolution hierarchy of the global coupled HadGEM3-GC3.1 model as used in CMIP6 HighResMIP experiments, Geosci. Model Dev., 12, 4999–5028, https://doi.org/10.5194/gmd-12-4999-2019, 2019.

Séférian, R., Nabat, P., Michou, M., Saint-Martin, D., Voldoire, A., Colin, J., Decharme, B., Delire, C., Berthet, S., Chevallier, M., Sénési, S., Franchisteguy, L., Vial, J., Mallet, M., Joetzjer, E., Geoffroy, O., Guérémy, J. F., Moine, M. P., Msadek, R., Ribes, A., Rocher, M., Roehrig, R., Salas-y Mélia, D., Sanchez, E., Terray, L., Valcke, S., Waldman, R., Aumont, O., Bopp, L., Deshayes, J., Éthé, C., and Madec, G.: Evaluation of CNRM Earth System Model, CNRM-ESM2-1: Role of Earth System Processes in Present-Day and Future Climate, Journal of Advances in Modeling Earth Systems, 11, 4182–4227, https://doi.org/10.1029/2019MS001791, 2019.

Seland, O., Bentsen, M., Olivié, D., Toniazzo, T., Gjermundsen, A., Graff, L. S., Debernard, J. B., Gupta, A. K., He, Y. C., Kirkeväg, A., Schwinger, J., Tjiputra, J., Schanke Aas, K., Bethke, I., Fan, Y., Griesfeller, J., Grini, A., Guo, C., Ilicak, M., Karset, I. H. H., Landgren, O., Liakka, J., Moseid, K. O., Nummelin, A., Spensberger, C., Tang, H., Zhang, Z., Heinze, C., Iversen, T., and Schulz, M.: Overview of the Norwegian Earth System Model (NorESM2) and key climate response of CMIP6 DECK, historical, and scenario simulations, Geoscientific Model Development, 13, 6165–6200, https://doi.org/10.5194/gmd-13-6165-2020, 2020.

Shao, Y., Raupach, M. R., and Leys, J. F.: A model for predicting aeolian sand drift and dust entrainment on scales from paddock to region, Australian Journal of Soil Research, 34, 309–342, https://doi.org/10.1071/SR9960309, 1996.

Shao, Y., Wyrwoll, K. H., Chappell, A., Huang, J., Lin, Z., McTainsh, G. H., Mikami, M., Tanaka, T. Y., Wang, X., and Yoon, S.: Dust cycle: An emerging core theme in Earth system science, Aeolian Research, 2, 181–204, https://doi.org/10.1016/j.aeolia.2011.02.001, 2011.

Shevliakova, E., Malyshev, S., Martinez-Cano, I., Milly, P. C. D., Pacala, S. W., Ginoux, P., Dunne, K. A., Dunne, J. P., Dupuis, C., Findell, K. L., Ghannam, K., Horowitz, L. W., Knutson, T. R., Krasting, J. P., Naik, V., Phillipps, P., Zadeh, N., Yu, Y., Zeng, F., and Zeng, Y.: The Land Component LM4.1 of the GFDL Earth System Model ESM4.1: Model Description and Characteristics of Land Surface Climate and Carbon Cycling in the Historical Simulation, Journal of Advances in Modeling Earth Systems, 16, e2023MS003 922, https://doi.org/https://doi.org/10.1029/2023MS003922, 2024.

Shinoda, M., Gillies, J. A., Mikami, M., and Shao, Y.: Temperate grasslands as a dust source: Knowledge, uncertainties, and challenges, Aeolian Research, 3, 271–293, https://doi.org/10.1016/j.aeolia.2011.07.001, 2011.

Sigmond, M., Anstey, J., Arora, V., Digby, R., Gillett, N., Kharin, V., Merryfield, W., Reader, C., Scinocca, J., Swart, N., Virgin, J., Abraham, C., Cole, J., Lambert, N., Lee, W. S., Liang, Y., Malinina, E., Rieger, L., Von Salzen, K., Seiler, C., Seinen, C., Shao, A., Sospedra-Alfonso, R., Wang, L., and Yang, D.: Improvements in the Canadian Earth System Model (CanESM) through systematic model analysis: CanESM5.0 and CanESM5.1, Geoscientific Model Development, 16, 6553–6591, https://doi.org/10.5194/gmd-16-6553-2023, 2023.

Sokolik, I. N., Darmenova, K., Huang, J., Kalashnikova, O., Kurosaki, Y., and Xi, X.: Examining changes in land cover and land use, regional climate and dust in Dryland East Asia and Their Linkages within the Earth System, in: Dryland East Asia: Land Dynamics amid Social and Climate Change, edited by Chen, J., Wan, S., Henebry, G., Qi, J., Gutman, G., Sun, G., and Kappas, M., chap. 9, pp. 183–211, DE GRUYTER, Berlin, Boston, ISBN 9783110287912, https://doi.org/10.1515/9783110287912.183, 2021.

Takemura, T., Egashira, M., Matsuzawa, K., Ichijo, H., O'Ishi, R., and Abe-Ouchi, A.: A simulation of the global distribution and radiative forcing of soil dust aerosols at the Last Glacial Maximum, Atmospheric Chemistry and Physics, 9, 3061–3073, https://doi.org/10.5194/acp-9-3061-2009, 2009.

Tatebe, H., Ogura, T., Nitta, T., Komuro, Y., Ogochi, K., Takemura, T., Sudo, K., Sekiguchi, M., Abe, M., Saito, F., Chikira, M., Watanabe, S., Mori, M., Hirota, N., Kawatani, Y., Mochizuki, T., Yoshimura, K., Takata, K., O'Ishi, R., Yamazaki, D., Suzuki, T., Kurogi, M., Kataoka, T., Watanabe, M., and Kimoto, M.: Description and basic evaluation of simulated mean state, internal variability, and climate sensitivity in MIROC6, Geoscientific Model Development, 12, 2727–2765, https://doi.org/10.5194/gmd-12-2727-2019, 2019.

Tegen, I., Harrison, S. P., Kohfeld, K., Prentice, I. C., Coe, M., and Heimann, M.: Impact of vegetation and preferential source areas on global dust aerosol: Results from a model study, Journal of Geophysical Research Atmospheres, 107, https://doi.org/10.1029/2001JD000963, 2002.

Tegen, I., Neubauer, D., Ferrachat, S., Drian, C. S. L., Bey, I., Schutgens, N., Stier, P., Watson-Parris, D., Stanelle, T., Schmidt, H., Rast, S., Kokkola, H., Schultz, M., Schroeder, S., Daskalakis, N., Barthel, S., Heinold, B., and Lohmann, U.: The global aerosol-climate model echam6.3-ham2.3 -Part 1: Aerosol evaluation, Geoscientific Model Development, 12, 1643–1677, https://doi.org/10.5194/gmd-12-1643-2019, 2019.

Textor, C., Schulz, M., Guibert, S., Kinne, S., Balkanski, Y., Bauer, S., Berntsen, T., Berglen, T., Boucher, O., Chin, M., Dentener, F., Diehl, T., Easter, R., Feichter, H., Fillmore, D., Ghan, S., Ginoux, P., Gong, S., Grini, A., Hendricks, J., Horowitz, L., Huang, P., Isaksen, I., Iversen, T., Kloster, S., Koch, D., Kirkevåg, A., Kristjansson, J. E., Krol, M., Lauer, A., Lamarque, J. F., Liu, X., Montanaro, V., Myhre, G., Penner, J., Pitari, G., Reddy, S., Seland, Stier, P., Takemura, T., and Tie, X.: Analysis and quantification of the diversities of aerosol life cycles within AeroCom, Atmospheric Chemistry and Physics, 6, 1777–1813, https://doi.org/10.5194/acp-6-1777-2006, 2006.

Van Noije, T., Bergman, T., Le Sager, P., O'Donnell, D., Makkonen, R., Gonçalves-Ageitos, M., Döscher, R., Fladrich, U., Von Hardenberg, J., Keskinen, J. P., Korhonen, H., Laakso, A., Myriokefalitakis, S., Ollinaho, P., Pérez Garciá-Pando, C., Reerink, T., Schrödner, R., Wyser, K., and Yang, S.: EC-Earth3-AerChem: A global climate model with interactive aerosols and atmospheric chemistry participating in CMIP6, Geoscientific Model Development, 14, 5637–5668, https://doi.org/10.5194/gmd-14-5637-2021, 2021.

Volodin, E. M.: Possible Climate Change in Russia in the 21st Century Based on the INM-CM5-0 Climate Model, Russian Meteorology and Hydrology, 47, 327–333, https://doi.org/10.3103/S1068373922050016, 2022.

Volodin, E. M. and Kostrykin, S. V.: The aerosol module in the INM RAS climate model, Russian Meteorology and Hydrology, 41, 519–528, https://doi.org/10.3103/S106837391608001X, 2016.

Woodward, S.: Modeling the atmospheric life cycle and radiative impact of mineral dust in the Hadley Centre climate model, Journal of Geophysical Research Atmospheres, 106, 18 155–18 166, https://doi.org/10.1029/2000JD900795, 2001.

Woodward, S.: Hadley Centre Technical Note 87 - Mineral dust in HadGEM2, Tech. rep., Met Office, Exeter, 2011.

Woodward, S., Sellar, A. A., Tang, Y., Stringer, M., Yool, A., Robertson, E., and Wiltshire, A.: The simulation of mineral dust in the United Kingdom Earth System Model UKESM1, Atmospheric Chemistry and Physics, 22, 14 503–14 528, https://doi.org/10.5194/acp-22-14503-2022, 2022.

Wu, C., Lin, Z., Liu, X., Li, Y., Lu, Z., and Wu, M.: Can Climate Models Reproduce the Decadal Change of Dust Aerosol in East Asia?, Geophysical Research Letters, 45, 9953–9962, https://doi.org/10.1029/2018GL079376, 2018.

Wu, C., Lin, Z., and Liu, X.: The global dust cycle and uncertainty in CMIP5 (Coupled Model Intercomparison Project phase 5) models, Atmospheric Chemistry and Physics, 20, 10 401–10 425, https://doi.org/10.5194/acp-20-10401-2020, 2020.

Xi, X.: On the Geomorphic, Meteorological, and Hydroclimatic Drivers of the Unusual 2018 Early Summer Salt Dust Storms in Central Asia, Journal of Geophysical Research: Atmospheres, 128, https://doi.org/10.1029/2022JD038089, 2023.

Xi, X. and Sokolik, I. N.: Seasonal dynamics of threshold friction velocity and dust emission in Central Asia, Journal of Geophysical Research: Atmospheres, 120, 1536–1564, https://doi.org/10.1002/2014JD022471, 2015a.

Xi, X. and Sokolik, I. N.: Dust interannual variability and trend in Central Asia from 2000 to 2014 and their climatic linkages, Journal of Geophysical Research: Atmospheres, 120, 12 175–12 197, https://doi.org/10.1002/2015JD024092, 2015b.

Xie, S., Terai, C., Wang, H., Tang, Q., Fan, J., Burrows, S., Lin, W., Wu, M., Song, X., Zhang, Y., Taylor, M., Golaz, J.-C., Benedict, J., Chen, C.-C., Feng, Y., Hannah, W., Ke, Z., Shan, Y., Larson, V., and Bader, D.: The Energy Exascale Earth System Model Version 3. Part I: Overview of the Atmospheric Component, Under Review, https://doi.org/10.22541/essoar.174456922.21825772/v1, 2025.

Yukimoto, S., Kawai, H., Koshiro, T., Oshima, N., Yoshida, K., Urakawa, S., Tsujino, H., Deushi, M., Tanaka, T., Hosaka, M., Yabu, S., Yoshimura, H., Shindo, E., Mizuta, R., Obata, A., Adachi, Y., and Ishii, M.: The meteorological research institute Earth system model version 2.0, MRI-ESM2.0: Description and basic evaluation of the physical component, Journal of the Meteorological Society of Japan, 97, 931–965, https://doi.org/10.2151/jmsj.2019-051, 2019.

Yumimoto, K., Tanaka, T. Y., Oshima, N., and Maki, T.: JRAero: The Japanese Reanalysis for Aerosol v1.0, Geoscientific Model Development, 10, 3225–3253, https://doi.org/10.5194/gmd-10-3225-2017, 2017.

Zender, C. S. and Kwon, E. Y.: Regional contrasts in dust emission responses to climate, Journal of Geophysical Research Atmospheres, 110, https://doi.org/10.1029/2004JD005501, 2005.

Zender, C. S., Bian, H., and Newman, D.: Mineral Dust Entrainment and Deposition (DEAD) model: Description and 1990s dust climatology, Journal of Geophysical Research: Atmospheres, 108, https://doi.org/10.1029/2002jd002775, 2003.

Zhang, J., Teng, Z., Huang, N., Guo, L., and Shao, Y.: Surface renewal as a significant mechanism for dust emission, Atmospheric Chemistry and Physics, 16, 15 517–15 528, https://doi.org/10.5194/acp-16-15517-2016, 2016a.

Zhang, K., Zhao, C., Wan, H., Qian, Y., Easter, R. C., Ghan, S. J., Sakaguchi, K., and Liu, X.: Quantifying the impact of sub-grid surface wind variability on sea salt and dust emissions in CAM5, Geoscientific Model Development, 9, 607–632, https://doi.org/10.5194/gmd-9-607-2016, 2016b.

Zhao, A., Ryder, C. L., and Wilcox, L. J.: How well do the CMIP6 models simulate dust aerosols?, Atmospheric Chemistry and Physics, 22, 2095–2119, https://doi.org/10.5194/acp-22-2095-2022, 2022.

Zomer, R. J., Xu, J., and Trabucco, A.: Version 3 of the Global Aridity Index and Potential Evapotranspiration Database, Scientific Data, 9, https://doi.org/10.1038/s41597-022-01493-1, 2022.

Zou, X. K. and Zhai, P. M.: Relationship between vegetation coverage and spring dust storms over northern China, Journal of Geophysical Research: Atmospheres, 109, https://doi.org/10.1029/2003jd003913, 2004.